THESIS

EVALUATING FILTRATION MEMBRANES AND DETECTION SYSTEMS FOR USE WITH VIRUS SURROGATES

Submitted by

Emily D. Stump

Graduate Degree Program in Bioengineering

In partial fulfillment of the requirements

For the Degree of Master of Science

Colorado State University

Fort Collins, Colorado

Summer 2010

COLORADO STATE UNIVERSITY

July 1, 2010

WE HEARBY RECOMMEND THAT THE THESIS PREPARED UNDER OUR SUPERVISION BY EMILY D. STUMP ENTITLED EVALUATING FILTRATION MEMBRANES AND DETECTION SYSTEMS FOR USE WITH VIRUS SURROGATES BE ACCEPTED AS FULFILLING IN PART THE REQUIREMENTS FOR THE DEGREE OF MASTER OF SCIENCE.

Committee on Graduate Work

_____
Sandra Quackenbush

_____
Matt Kipper

_____
John Pellegrino

_____
Advisor: S. Ranil Wickramasinghe

_____
Director: Susan James

ABSTRACT OF THESIS

EVALUATING FILTRATION MEMBRANES AND DETECTION SYSTEMS FOR USE WITH VIRUS SURROGATES

Virus filtration membranes are used to provide size exclusion removal of viruses during the purification of biopharmaceutical products. This viral clearance is required by regulatory agencies to ensure the safety of patients by preventing contamination of product by adventitious or endogenous virus. Viral clearance studies are often laborious, expensive, and require highly trained personnel. Detection and quantification of virus using standard assays has restrictions in terms of limit of detection, extraneous contamination and false positives. Moreover, biosafety for personnel and the environment is always a concern when working with live virus. In order to avoid the hazards of live, adventitious virus, bacteriophages have been used previously as virus surrogates (Aranha-Creado & Brandwein, 1999). While the health threat associated with using live viruses is eliminated using bacteriophages as surrogates, the detection systems and quantitative assays are still laborious and difficult. Development of a non-biological system to simulate and quantify virus particles could reduce the time taken to perform viral clearance tests; reduce development costs; reduce the risk to personnel performing the tests; and lead to more reliable data, since a non-biological system will reduce variability in assays. Here we develop a prototype of a novel, gigantic magnetoresistive (GMR) detection system for magnetic virus surrogates. In addition, we investigate various polymeric membranes for their ability to reject virus. Results will be used as a benchmark for evaluating the behavior of a future, superparamagnetic virus surrogate.

GMR-based technology has increasingly been on the rise since the 2007 Nobel Prize in physics was awarded to Albert Fert and Peter Grünberg for its discovery. GMR sensors show potential for being extremely sensitive, inexpensive, and flexible devices for use in biodetection assays. Compared to the current magnetic detection technology of the superconducting quantum interference device (SQUID), which requires complex instrumentation and qualified users, GMR technologies can be fabricated in such a

manner so as to be applied to lab-on-chip systems. Here we discuss the sensor design and fabrication. Initial measurements indicate that 10^4 iron oxide nanoparticles, approximately 20nm in diameter, can be detected in 0.5µl of solution.

Various virus filters as well as ultrafiltration membranes were challenged with feed streams spiked with high concentrations of minute virus of mice (MVM) in the presence and absence of 1% bovine serum albumin (BSA) (w/v). Changes in permeate flux with filtrate volume were determined in conjunction with changes in rejection of parvovirus. Decrease in permeate flux resulting from fouling of BSA was evaluated for its effect on virus rejection. The results, which compare the performance of virus filtration and similar ultrafiltration membranes, provide insights into the comparison of live virus with future virus surrogates.

Emily D. Stump
Graduate Degree Program in Bioengineering
Colorado State University
Fort Collins, CO 80523
Summer 2010

Acknowledgements

I would like to thank the Membrane Applied Science and Technology (MAST) Center for providing funding for this research. Thank you to Dr. Irv Joffee and Dr. Gabe Tkacik of Pall and Millipore, respectively, for providing the membranes and additional mentoring for this project.

Acknowledgements also go to the National Institute of Standards and Technology, Electromagnetics Division, including Stephen Russek, Justin Shaw, Ranko Heindel, and Robert Usselman, for their integral part in this project.

I would also like to thank Dr. S. Ranil Wickramasinghe for serving as my advisor, and Dr. John Pellegrino for providing mentoring and oversight. Thank you to Dr. Sandra Quackenbush and Dr. Matt Kipper for serving on my committee.

I would like to acknowledge Dr. Jon Carlson for allowing this research to be conducted in his lab. Additionally, Justin Weaver, David Grzenia, Xinying Wang, and Hailey Cutler have provided great assistance with conducting this research.

TABLE OF CONTENTS

Signature Page ii
Abstract iii
Acknowledgements v
Table of Contents vi
List of Figures vii
List of Tables viii
Chapter 1: Literature Review 1
1.1 Introduction 1
1.2 Virus Clearance 3
1.2.1 Regulatory Involvement 3
1.2.2 Sources of Viral Contamination 4
1.2.3 Prevention 7
1.2.4 Validating Viral Clearance 8
1.2.5 Minute Virus of Mice (MVM) 10
1.3 Membranes 11
1.3.1 Ultrafiltration 12
1.3.2 Virus Filtration 13
1.3.3 Concentration Polarization and Fouling 14
1.4 Gigantic Magnetoresistance (GMR) 16
Chapter 2: Experimental Methods (Membrane Filtration) 18
2.1 Introduction 18
2.2 Cell Culture 18
2.3 Virus Propagation 19
2.4 Filtrate 20
2.5 Filtration 20
2.6 Virus Quantification 22
2.7 Bovine Serum Albumin (BSA) Assay 23
2.8 Critical Point Drying for Scanning Electron Microscopy 23
Chapter 3: Results and Discussion 25
3.1 Membrane Evaluation 25
3.2 Virus/Protein Rejection and Fouling 29
Chapter 4: Conclusions 38
Chapter 5: Future Work 40
References 41
Appendix I: Real Time PCR Data 46
Appendix II: Gigantic Magnetoresistive (GMR) Sensor 58
Appendix III: Constant Flux Filtration 73

LIST OF FIGURES

Figure 1: Schematics of NFF and TFF 14
Figure 2: Experimental Setup 21
Figure 3: FESEM Images of Virus Filtration Membranes 26
Figure 4: FESEM Images of Ultrafiltration Membranes 27
Figure 5: Pure Water Fluxes at 0.2MPa 29
Figure 6: Fluxes Obtained for Filtration of Feed Streams Containing MVM in the Absence of Protein 30
Figure 7: Fluxes Obtained for Filtration of Feed Streams Containing MVM and 1% (w/v) BSA 31
Figure 8: Log Reduction of Virus from Feed Streams Spiked with MVM not Containing Protein 33
Figure 9: Log Reduction of Virus from Feed Streams Spiked with MVM and 1% (w/v) BSA 34
Figure 10: Comparison of Water Flux Before Filtration and After Filtration with 1% (w/v) BSA 35
Figure 11: BSA Transmission 37
Figure 12: GMR Assay Design 59
Figure 13: GMR Scanner Design 60
Figure 14: MNPVS Assay Prototype 68
Figure 15: MNPVS Scanner Prototype 69
Figure 16: Atomic Force Micrographs 70
Figure 17: Voltage Output During Application of Various Concentrations of Iron Oxide Nanoparticles 71
Figure 18: Voltage Output During Application of 2×10^8 Iron Oxide Nanoparticles 71
Figure 19: Log Virus Removal for 30 PSI Constant Pressure Filtration and Constant Flux Filtration of Feed Streams Spiked with MVM Not Containing Protein 74
Figure 20: Transmembrane Pressures for Constant Flux Filtration of Feed Streams Spiked with MVM Not Containing Protein 75
Figure 21: Comparison of Transmembrane Pressure Before Filtration and After Filtration with Feed Streams Spiked with MVM Not Containing Protein 76

LIST OF TABLES

Table 1: Viral Contamination Related to Cell Lines and Human and Animal Biologicals 6
Table 2: Membranes 21
Table 3: Overall BSA Transmission for Feed Streams Containing MVM and 1% (w/v) BSA 36

Chapter 1.

Literature Review

1.1 Introduction

Many pharmaceutical products are required to be tested and evaluated for viral safety before approval to market. These products include monoclonal antibodies, hormones, vaccines, and recombinant proteins. Viral contamination poses a severe risk on the patient and can arise from a variety of sources. Such sources include the biological systems that the product is produced in (such as cell lines), raw materials (such as media components), or introduction of adventitious virus during production from the manufacturing environment, personnel, etc. Contaminations by organisms such as bovine viral diarrhea virus, epizootic hemorrhagic disease virus, minute virus of mice, hepatitis B virus, SV40, and avian leukosis virus have previously been reported (Aranha-Creado & Brandwein, 1999; Merten, 2002; Erickson, Bolin, & Lundgraf, 1991; Rabenau, et al., 1993; Garnick, 1996; Fox, Manso, Penna, & Para, 1942; Shah & Nathanson, 1976; Harris, et al., 1966).

FDA guidelines suggest that in order to confidently determine the absence of virus in biotechnology products, a combination approach is necessary. Viral assay testing should be utilized, and an overall demonstration that the production process and further purification methods are capable of removing and/or inactivating virus is required. Viral clearance studies are performed using "relevant" viruses (viruses that are likely to contaminate the cell substrate), specific "model" viruses (closely related to the suspected, contaminating virus), or nonspecific "model" viruses (used to characterize the capacity of the manufacturing process to remove or inactivate viruses in general) (FDA, 1998).

Viral clearance studies, that assess the process step(s) which are effective in removing viruses, call for the intentional addition of a known titer of virus (or virus surrogate) to bulk material and subsequent evaluation of the effectiveness of the process to remove that known quantity of contaminant. This removal of virus is often performed via a filtration process near the end of purification (Wickramasinghe, Han, Carlson, & Powers, 2004). However, extreme cautions must be taken when working with live viruses and bringing live viruses into a pharmaceutical testing facility. Certain "relevant" or "model" viruses may pose health

hazards to personnel performing the clearance studies. Additionally, current Good Manufacturing Practices (cGMPs) mandated by the Food and Drug Administration for production of pharmaceutical products, would be put at risk if any virus was introduced to the actual production facility. Viral clearance studies are therefore required to be performed in a separate laboratory having separate air handling units from the product facility (FDA, 1998).

In order to avoid the hazards of live, adventitious virus, bacteriophages have previously been used as virus surrogates. While the health threat associated with using live viruses is eliminated using bacteriophages as surrogates, the detection systems and quantitative assays are still laborious and difficult. The development of a magnetic detection system for use with superparamagnetic nanoparticles that simulate of 20nm parvovirus will decrease the time it takes to perform testing and can be designed as a relatively simple and flexible system. Magnetoresistive (MR) sensors are widely applied in the data storage market as read heads in hard disk drives. Their ability to detect very weak magnetic fields (down to the nT scale) at room temperature has lead to their growing popularity over other methods such as the Super Conducting Quantum Interference Device (SQUID). Magnetoresistive devices used for biomolecular recognition involving magnetically labeled target molecules, have emerged as an application with the potential to detect single molecules or particles (Li, Sun, Wilson, White, Pourmand, & Wang, 2006; Freitas, Ferreira, Cardoso, & Cardoso, 2007). This work discusses the sensor design and fabrication. Initial measurements indicate that 10^4 iron oxide nanoparticles, approximately 20nm in diameter, can be detected in 0.5µl of solution. The use of a sensitive and flexible sensor in quantifying virus surrogates will serve as a means to increase limit of detection and decrease variability in live viral assays.

Effective virus filtration membranes are designed to provide high levels of viral clearance while ensuring adequate transmission of the desired protein, as well as good capacity. The overall performance of virus filters is primarily dominated by membrane fouling, which can alter flux, capacity, and transmission characteristics (Bakhshayeshi & Zydney, 2008). Additionally, virus filters must be manufactured specifically to eliminate all macro-defects. This has led to the use of composite (multi-layer) membrane structures that provide the required combination of virus retention and mechanical stability. Studies of

protein fouling, compaction, and permeability effects on virus membranes have previously been conducted, however, these studies have not provided data specifically on virus rejection as a function of those parameters (Bohonak & Zydney, 2005; Syedain, Bohonak, & Zydney, 2006).

In the following work, the performance of viral filtration membranes has been compared in tandem to that of ultrafiltration membranes. Six commercially available membranes were challenged with feed streams spiked with high concentrations of minute virus of mice (MVM) in the presence and absence of 1% bovine serum albumin (BSA) (w/v). All asymmetric membranes were operated in normal flow, constant pressure mode with the filtration surface facing away from the feed stream, as is industrial practice for virus filtration. Changes in permeate flux with respect to variable filtrate volume were determined in conjunction with changes in rejection of parvovirus. Decrease in permeate flux resulting from fouling of BSA was also evaluated for its effect on virus rejection. The evaluation of the performance of various different filters can serve as a basis for comparison in the study of virus surrogates used in membrane integrity tests and viral clearance studies.

1.2 Virus Clearance

1.2.1 Regulatory Involvement

The Food and Drug Administration (FDA) and European Medicines Agency (EMEA) require manufacturers of biologics to assess and reduce the risk of introducing a viral contaminant into their products. This is not only for the health of the patient, but also for the health of the laboratory and manufacturing personnel. In order to accomplish this assessment, the FDA produces guidance documents to publicize new or changed regulatory expectations for the first time. These guidance documents are not mandated by law, but rather they represent the FDA's current interpretation of a specified topic relating to the laws of the Code of Federal Regulations (CFR). The International Conference on Harmonization of Technical Requirements for Registration of Pharmaceuticals for Human Use (ICH) was formed in 1990 with the goal of unifying drug approval processes in the United States, Europe, and Japan (ICH, 2008). In minimizing and harmonizing each participating countries regulations, not only will drug products transition to market more quickly, they will also reach a larger market, without compromising high standards of

safety, quality, and efficacy. The guidance document, Q5A: Viral Safety Evaluation of Biotechnology Products Derived from Cell Lines of Human or Animal Origin, has become a crucial reference document for the biopharmaceutical industry in terms of viral clearance and safety to personnel, the environment, and patients.

From this document, three methods to control potential viral contamination of biologics have been recommended. These methods involve a combination of testing cell lines and other raw materials for the absence of viruses, evaluating the production processes itself as a mechanism to eliminate viruses, and finally, testing product at various steps of production for the absence of viruses (FDA, 1998). Additionally, other guidance documents outline specific viral safety tests that must be performed at various stages of production on raw materials, in-process material, or final products. The type of sample to be tested for viral safety dictates which regulatory guidance should be referenced (Nims R. W., Detection of Adventitious Viruses in Biologicals - A Rare Occurence, 2006). The testing of raw materials follows methods outlined in the CFRs and Q5A, among others. Cell line characterization is driven by another specific guidance, while bulk harvest testing, is governed by other guidances that may be specific to the final product, such as those developed for monoclonal antibody products (FDA/CBER, 1993; FDA/CBER, 1997). These documents provide manufacturers of biotechnology products the framework for ensuring patient safety above all else.

1.2.2 Sources of Viral Contamination

Virus can be introduced into a biological product in a number of different ways. Contamination may arise from the original cell lines or by introduction of adventitious virus during the production process, either by raw materials or a breakdown in the process itself (Merten, 2002; Aranha-Creado & Brandwein, 1999; FDA, 1998). The following are examples of viral contamination in biological products from the aforementioned routes.

Although primary cell cultures derived from animal tissues are rarely used for the production of biological products for human use today, they are used in veterinary products, and they were used for the production

of the polio vaccine in the 1950s and 1960s (Merten, 2002; Shah & Nathanson, 1976). In 1960, it was discovered that both the Salk (inactivated) and Sabin (live attenuated) poliovirus vaccines were contaminated with simian virus 40 (SV40) (Sweet & Hilleman, 1960). SV40 persists in immunocompromised monkeys causing a latent infection of the kidneys. The SV40 virus went undetected during initial vaccine production as it did not display cytopathic effects in the monkey kidney cells and grows more slowly than poliovirus. It is thought that the formaldehyde inactivation treatment during Salk vaccine production was unsuccessful in eliminating SV40 virions, while there was no inactivation treatment for the Sabin vaccine (Carbone, Rizzo, & Pass, 1997).

Animal derived materials, such as serum, constitute the primary reason for viral contamination (Nims R. , 2009). Other animal derived products such as trypsin, other enzymes, and amino acids, also pose the same risks. A recent contamination at Genzyme Corporation halted production, which impacted patient supplies of two therapeutic products, Cerezyme® and Fabrazyme®. The manufacturing facility discovered that a strain of vesivirus had been introduced in their Chinese hamster ovary (CHO) cell line through a nutrient used in the manufacturing process (Genzyme Corporation, 2009).

While the FDAs current Good Manufacturing Practice (cGMP) guidelines specify requirement for the health, hygiene, and protective equipment and clothing of manufacturing personnel, contamination can also occur during cell and medium handling. A breakdown in cGMP could also occur via incomplete pest and rodent control, or other equipment and procedural failures.

Other methods of viral contamination include use of a contaminated reagent such as a monoclonal antibody affinity column or a contaminated excipient during formulation. Additionally, the use of a virus to establish a cell line or using a virus to induce expression of specific genes encoding a protein of interest can lead to viral contamination (FDA, 1998). Hybridoma cell lines can be established by fusing human Epstein-Barr virus (EBV) transformed lymphblastoid cells with mouse plasmacytomas. These cells have the potential for producing infectious EBV (Merten, 2002). Additionally, CHO cells and murine hybridoma cells are known to contain endogenous retroviruses and produce retroviral particles. Finally,

Adeno-Associated virus (AAV) is known to infect cells, but cannot replicate without the assistance of another virus, further complicating potential routes of contamination (Merten, 2002). Table 1 provides further examples of published viral contamination incidents related to cell lines and human and animal biologicals.

Table 1. Viral Contamination Related to Cell Lines and Human and Animal Biologicals

Virus	Substrate	Source	Product or Company	Reference
HBV	Undisclosed	Human serum used as excipient	Yellow fever vaccine	(Fox, Manso, Penna, & Para, 1942)
SV40	Rhesus monkey kidney cells	Endogenous infection of monkeys	Salk and Sabin poliovaccines	(Sweet & Hilleman, 1960)
ALV	Hens eggs or chick embryo cell cultures	Endogenous infection of animals	Live virus vaccines against yellow fever (YFS 2) and measles (MV 16)	(Harris, et al., 1966)
MVM	BHK cells	Contaminated FCS	Wellcome Foot-and-Mouth Disease Vaccine Laboratory	(Nettleton & Rweyemamu, 1980)
Ovine Pestivirus	Undisclosed	Unknown	Live virus vaccine against pseudorabies	(Vannier, Leforban, Carnero, & Cariolet, 1988)
LCMV, MVM, Sendai virus, EDIM, LDHV, Porcine parvovirus, BVDV	Various production cell banks	Unknown	Undisclosed	(Moore, 1992)
Bluetongue Virus	Undisclosed	Unknown	Multivalent modified live vaccine against canine distemper virus, adenovirus, and parvovirus vaccines	(Akita, Ianconescu, MacLachlan, & Osburn, 1994)
BVDV	Undisclosed	Contaminated FBS	2 measles-mumps-rubella combined vaccines, 2 monovalent vaccines against mumps and rubella	(Harasawa & Tomiyama, Evidence of Pestivirus RNA in Human Virus Vaccines, 1994)
BVDV	Human lymphoblast and fibroblast cell cultures	Contaminated FBS	Human rIFN-α and rIFN-β	(Harasawa & Sasaki, Sequence Analysis of the 5' Untranslated Region of Pestivirus RNA Demonstrated in Interferons for Human Use, 1995)

Table 1, continued.

Virus	Substrate	Source	Product or Company	Reference
BVDV	HmLu-1 cells, Chick embryo cell culture, Porcine testis cells, Porcine kidney cells, Guinea-pig kidney cells, Quail embryo cell culture	Contaminated FBS	Live virus vaccines against Akabane disease, Ibaraki disease, infectious bovine rhinotracheitis, porcine parvovirus infection, transmissible gastroenteritis, and Japanese encephalitis	(Harasawa, Adventitious pestivirus RNA in live virus vaccines against bovine and swine diseases, 1995)
EHDV	CHO Cells	Contaminated FBS	Bioferon GmbH & Co. Recombinant protein for phase I clinical trials	(Burstyn, 1996)
MVM	CHO Cells	Contaminated raw material	Pulmozyme®, Genentech	(Garnick, 1996)
Vesivirus 2117	CHO cells	Contaminated FBS	Boehringer Ingelheim Pharmaceuticals	(Oehmig, Buttner, Weiland, Werz, Bergemann, & Pfaff, 2003)
Reovirus	Unprocessed bulk harvest (CHO cells)	Contaminated FBS	Undisclosed	(Nims R. W., Detection of Adventitious Viruses in Biologicals - A Rare Occurence, 2006)
CVV	CHO cells	Contaminated FBS	Undisclosed	(Nims, et al., 2008)
Vesivirus 2117	CHO cells	Contaminated raw material	Cerezyme® and Fabrazyme®, Genzyme	(Genzyme Corporation, 2009)

Abbreviations: HBV, Hepatitis B Virus; SV40, Simian virus 40; ALV, Avian Leukosis Virus; MVM, Minute Virus of Mice; BHK, Baby Hamster Kidney; FCS, Fetal Calf Serum; LCMV, Lymphocytic Choriomeningitis Virus; EDIM, Epizootic Diarrhea of Infant Mice Virus; LDHV, Lactic Dehydrogenase Virus; BVDV, Bovine Viral Diarrhea Virus; FBS, Fetal Bovine Serum; IFN, Interferon; EHDV, Epizootic Hemorrhagic Disease Virus; CHO, Chinese Hamster Ovary; CVV, Cache Valley Virus.

1.2.3 Prevention

Viral contamination can be prevented, and is required to be prevented, in a number of different ways. The first, and most obvious prevention method is to eliminate animal derived materials from a production process altogether. However, this may not always be possible. When animal derived materials must be used, the first safety measure is to implement testing procedures for those materials that includes adventitious viruses. These tests apply to raw materials as well as production cell banks. Additionally, animal derived materials should be sourced to their country and tissue of origin, and other safety measures

such as heat inactivation and gamma irradiation should be employed, where possible. Secondly, the production process itself must be evaluated for its capacity to eliminate virus. A process that inherently has high levels of virus clearance or inactivation is desirable (discussed in detail in the next section). Additionally, disposable technology, which eliminates contamination from vessel to vessel, is becoming more prevalent. Lastly, final products as well as intermediates within the process should be tested for virus at frequent intervals.

All three of these strategies must be implemented together in order to adequately ensure the safety of products (Minor, 1996). The systems available for viral screening have their limitations. For example, a cell culture system can only detect those viruses which are able to grow in those cells, and grow in those cells at an observable rate. Sample size and frequency for testing a raw material like FBS, for example, may not be sufficient to detect extremely low levels of virus, and virus which is only present in certain fractions of a particular large scale lot.

1.2.4 Validating Viral Clearance

Viral clearance studies are performed in order to evaluate various different steps in the manufacturing process for their ability to inactivate or remove viruses thereby providing an estimate of the overall level of virus reduction obtained by the process itself. These studies are performed by intentionally adding known quantities of virus to representative feed streams at different stages of the process and subsequently proving virus removal or inactivation. Current Good Manufacturing Practices (cGMPs) mandated by the Food and Drug Administration for production of pharmaceutical products would be put at risk if any virus was introduced to the actual production facility. Viral clearance studies are therefore required to be performed in a separate laboratory from the production facility (FDA, 1998).

Virus retention is quantified by a Log Reduction Value (LRV), which is the logarithm (base 10) of the ratio, S, of the viral concentration in the feed to that in the filtrate:

$$LRV = \log_{10} S \qquad (1)$$

(van Reis & Zydney, 2007; Brorson, et al., 2008). Evaluating viral clearance on a logarithmic scale mathematically shows a large reduction in virus; however, no method of quantifying virus could guarantee a reduction of virus to zero. Using filtration as a mechanism for viral clearance typically provides a minimum of a 4 $\log_{10}$ reduction in viral load. An ideal estimate for overall virus reduction factor for a unit operation is approximately a 12-18 $\log_{10}$ reduction. In other terms, regulatory guidance suggests that less than one virus particle per million doses be used to calculate the overall LRV (FDA, 1998; Kern & Krishnan, 2006). This value is calculated based on recommendations from the FDA to estimate the concentration of virus in a cell culture harvest to be 10^6/ml. Assuming a viral clearance factor of greater than 10^{15}, and a hypothetical volume of 10^3 ml of harvest to create a single dose of a product, virus particles per dose is calculated as follows:

$$\frac{\left(10^6 \text{ virus} \frac{\text{units}}{\text{ml}}\right) \text{x} \left(\frac{10^3 \text{ml}}{\text{dose}}\right)}{\text{Clearance factor} > 10^{15}} = < 10^{-6} \frac{\text{particles}}{\text{dose}} \qquad (2)$$

Virus, however, cannot be grown to high enough titers to be able to demonstrate this level of clearance. In order to overcome this obstacle, LRV should be determined after each process step, compared with each other, and then summed to produce an overall viral clearance level.

Filtration processes are scaled down in a linear fashion and typically represent "worst case" scenarios for viral clearance. It is important to demonstrate that the scaled down process represents, as closely as possible, the large scale process. This is accomplished by using similar pH, temperatures, concentrations (salt, protein, product, etc.), linear flow rate, contact time, pressures, ratio of volume to membrane surface area, and so on (FDA, 1998). However, in order to operate under worst-case situations, the design space for the validation studies should also include challenge parameters such as high protein concentration (Brorson, et al., 2008).

The choice of virus(es) for use in validation studies is quite complex. Three categories have been outlined by the FDA: Relevant, specific model, or nonspecific model viruses (FDA, 1998). Relevant viruses are meant to be the virus (or same species of virus) that has previously been identified to contaminate a cell substrate or other reagents or materials used in the production process. For example, bovine viral diarrhea

virus is a relevant virus for the contamination of FBS. Specific model viruses are used when a relevant virus is not available or cannot be grown to high enough titers to perform validations studies. These viruses are closely related to the relevant virus, where similar physical and chemical properties are conserved. For example, a murine leukemia virus is a specific model virus for cell lines derived from murine species, which may produce endogenous retrovirus particles. Nonspecific model viruses are used to evaluate viral clearance of the production process by and large. Nonspecific model viruses typically represent a broad range of physicochemical properties, and exhibit resistance to inactivation or removal techniques. The choice of virus should also reflect practicality in regard to propagation of virus, viral assay methods, and laboratory and personnel safety (Brorson, et al., 2008). Regardless of the choice of virus, a justification in line with the guidance documents, type of process, and substrates is required.

1.2.5 Minute Virus of Mice (MVM)

For these experiments, MVM was chosen as a nonspecific model virus. As mentioned previously, MVM has been associated with large scale contaminations related to biotechnology products (Garnick, 1996). Additionally, FDA recommends the use of animal parvovirus as a nonspecific model virus that exhibits a range of physicochemical structures in order to characterize the capacity of the manufacturing process to remove and/or inactivate viruses in general (FDA, 1998). Parvoviruses are very small, typically 18-26nm in diameter, non-enveloped, icosahedral viruses containing a single stranded DNA genome (Strauss & Strauss, 2002). Their minute size not only gives rise to the name, minute virus of mice, it also causes removal of the virus via size exclusion to be challenging. Parvoviruses, however, are known to be resistant to inactivation via physicochemical treatments such as heat, pH, and denaturing agents. Boschetti, et al. showed MVM to be resistant to low pH (pH 4 for greater than 6 hours), as well as high pH ($\leq$11.8), and steam treatment ($\leq$90°C) (Boschetti, Niederhauser, Kempf, Stühler, Löwer, & Blümel, 2004; Boschetti, Wyss, Mischler, Hostettler, & Kempf, 2003). These inactivation steps, which are typically employed as part of the overall purification train in a manufacturing process, are more effective at inactivating enveloped viruses (Eterpi, McDonnell, & Thomas, 2009; Furuya, et al., 2006). MVM, therefore, is an excellent model virus for filtration experiments, where pore size and porosity are influential factors in effective viral clearance.

Additionally, MVM is classified as a biosafety level 2 (BSL 2) agent and therefore requires minimal containment, such as use of a biological safety cabinet, autoclave, and proper personal protective equipment (ATCC, 2010). Due to the species and tissue tropism exhibited by parvoviruses, there were few health risks to personnel working with this mouse parvovirus (Strauss & Strauss, 2002).

1.3 Membranes

Membranes are employed in numerous technical industries such as water purification, food, pharmaceuticals, medical devices, chemicals, and gas. They are composed of a variety of different materials depending on their application, including organic polymers, inorganic materials (oxides, ceramics, and metals), mixed matrix, and composite materials (Ulbricht, 2006). Membranes comprised of organic polymers are most frequently used, and will be the focus of this research. Filters used for the separation of liquids are classified according to their selective barrier, structure, morphology, and material. Pressure driven transport through porous membranes is based upon size exclusion, where permeability and selectivity are primarily affected by pore size and the size of the particles or molecules in the feed stream. Additionally, fouling of the membrane due to interactions of molecules in the feed stream and the membrane itself significantly affects the performance of filtration (i.e., flux and capacity) (Susanto & Ulbricht, 2008).

Efficient membrane processes must maximize their selectivity, productivity, and capacity. The selectivity of a membrane is its ability to reject unwanted materials, while maximizing the passage of the product. Selectivity for pressure driven membrane processes is defined as:

$$S = \frac{C_f}{C_F} \tag{3}$$

where S is the solute sieving coefficient, and C_f and C_F are the solute concentrations in the filtrate and feed solutions, respectively (van Reis & Zydney, 2007).

Productivity is the volumetric filtrate flux, which is affected in large part by fouling mechanisms such as concentration polarization and pore blockage. Flux is related to the membrane permeability, and can be described by the following equation:

$$L_p = \frac{\mu J}{\Delta P} \quad (4)$$

where L_p is the permeability, μ is the solution viscosity, J is the filtrate flux (volumetric flow rate per unit membrane area), and ΔP is the transmembrane pressure difference (van Reis & Zydney, 2007).

The capacity of a membrane is the volume of feed that can be processed per unit membrane area before extreme flux decline occurs and the membrane must be replaced. Capacity can loosely be defined as the point at which the filtrate flux or pressure decreases below a predetermined value that is desirable for a particular application.

1.3.1 Ultrafiltration

Ultrafiltration (UF) membranes typically have pore sizes in the range of 10 to 1000Å, thicknesses varying from 0.1 to 1µm, and an asymmetric structure (Kulkarni, Funk, & Li, 2001). Anisotropic, or asymmetric, membranes are designed to have a mechanically stable, thick, porous structure used as a barrier for the thin, porous selective skin that serves to provide size exclusion. This asymmetry reduces the thickness of the selective barrier (or skin), as well as increases permeate flux. The pore size distribution for UF membranes tends to be quite broad, which results in limited size selectivity (Susanto & Ulbricht, 2008). UF membranes, however, are not described by their pore size. Nominal molecular weight cutoff (NMWCO), which is defined as the smallest molecular weight species for which the membrane has greater than 90% rejection, is used to classify these membranes. The MWCO and performance characteristics of UF membranes are strongly affected by the composition of the feed stream, operating conditions, and orientation of the membrane.

UF membranes are designed to operate around 0.2 to 1.0 MPa, except in the case of high pressure tangential flow filtration (HPTFF), where operating ranges can reach 2.5 to 3.0 MPa (Kulkarni, Funk, & Li, 2001). Tangential flow filtration (TFF) is the preferred method for use with ultrafiltration membranes. In

TFF, the feed stream runs parallel to the membrane, while the permeate is driven perpendicular to the membrane (refer to Figure 1). This orientation helps to prevent rejected molecules from building up on the membrane surface when the selective barrier is facing the feed stream (van Reis & Zydney, 2007).

1.3.2 Virus Filtration

Virus filtration membranes have pore sizes between 20 and 70nm (van Reis & Zydney, 2007). Virus filters, however, must not contain any macro defects. A very narrow pore size distribution is required in order to completely reject virus particles (Kern & Krishnan, 2006). The pore size is determined by the type of virus that is to be rejected. For example, retrovirus membranes are designed to reject retroviral particles greater than approximately 50nm, which is significantly larger than parvovirus particles in the 20nm range. Separation efficiency of the product of interest from other impurities, however, is greatest when there is at least a ten-fold difference in the sizes of the species being separated (Kulkarni, Funk, & Li, 2001), so designing virus filters that allow 98% of protein transmission can be difficult.

Virus filters are currently designed either as symmetric or asymmetric structures and can be run under conditions of constant pressure or constant flux. Constant flux filtration, however, often leads to rapid fouling of the membrane and high pressures required to maintain the flux (Ho & Zydney, Transmembrane Pressure Profiles During Constant Flux Microfiltration of Bovine Serum Albumin, 2002). Refer to Appendix III for additional information.

Previously, virus filters, like ultrafiltration membranes, were designed to be operated in TFF mode (DiLeo, Allegrezza, & Builder, 1992). Normal flow filtration (NFF), however, has recently emerged as a desirable mechanism for virus filtration (van Reis & Zydney, 2007; Wickramasinghe S. R., 2008). Employing TFF as a filtration mechanism incurs high costs related to cleaning validation for reusable membranes. The single use, disposable nature of filters used in NFF makes them a more simplistic and low cost alternative. Also, in contrast to ultrafiltration membranes, the asymmetric filters tend to be operated with their selective barrier facing away from the feed stream (Brough, Antoniou, Carter, Jakubik, Xu, & Lutz, 2002). In doing

so, the macroporous base serves as an inline pre-filter to eliminate larger aggregates before they reach the virus retentive skin layer.

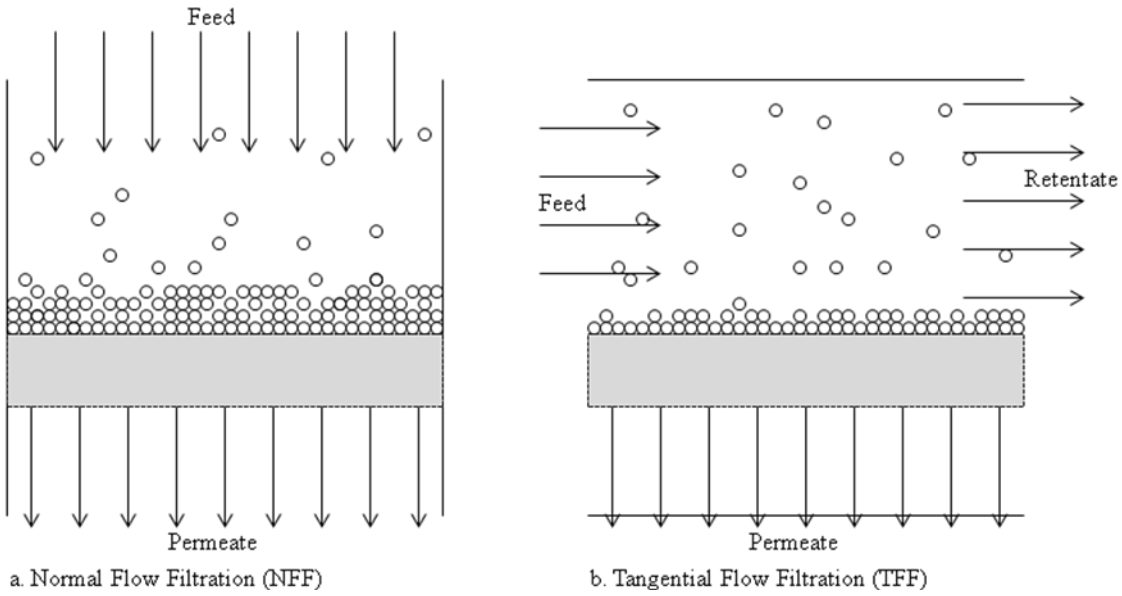

Figure 1. Schematics of NFF and TFF

Virus retention is primarily attributed to size exclusion which is only a function of the membrane pores, and is not affected by intrinsic factors such as feed stream and operating conditions. These parameters, however, do play a role in virus reduction when pore sizes exceed the size of the virus. Wickramasinghe, et al., for example, have shown increased clearance of MVM and Murine Leukemia Virus (MLV) in microfiltration by flocculation with a cationic polyelectrolyte (Wickramasinghe, Han, Carlson, & Powers, 2004; Akeprathumchai, Han, Wickramasinghe, Carlson, Czermak, & Prei, 2004). van Voorthuizen et al. showed that hydrophobic and electrostatic interactions among virus particles and membranes also played an important role in virus rejection (van Voorthuizen, Ashbolt, & Schäfer, 2001). Virus adsorption to membranes can be achieved through a variety of mechanisms including charge, van der Waals interactions hydrogen bonding, steric hindrance, and through the use of adsorptive membranes (Brorson, et al., 2008). While these factors are important to consider in virus filtration operations, size exclusion still remains the most robust, scalable, and efficient mechanism to achieve viral clearance.

1.3.3 Concentration Polarization and Fouling

Concentration polarization is a phenomenon common among pressure driven filtration processes. Molecules that are rejected by the membrane, build up at its surface to a concentration of c_w. When this value reaches its maximum due to mass transfer limitations, the membrane experiences a higher feed side concentration resulting in reduced flux and rejection (Kulkarni, Funk, & Li, 2001; van Reis & Zydney, 2007). Concentration polarization is dependent upon pressure, temperature, and feed concentration. Running membrane processes in TFF mode decrease the effects of concentration polarization by producing high shear rates on the membrane surface, preventing build up of solutes.

Fouling is caused when the feed stream deposits its components directly on the membrane surface or within the membrane pores. Fouling, as opposed to concentration polarization, is dependent upon time. The concentration, c_w, of solutes at the membrane surface can increase to the point where a cake layer is formed, thereby also decreasing flux due to a hydraulic resistance to flow. Molecules build up in the membrane pores as a result of pore geometry (tortuosity) or interactions of the molecules with the pore walls. When fouling occurs, rejection either remains constant or can increase.

Fouling in constant pressure normal flow filtration can be described by four pore blocking models: standard blocking, complete blocking, intermediate blocking, and cake filtration (van Reis & Zydney, 2007; Loh, et al., 2009; Hermia, 1982). Standard blocking occurs when a decrease in pore diameter is observed due to foulants depositing along pore walls. While the pore size effectively decreases, the number of pores per unit area remains the same. Complete blocking, on the other hand, is when material blocks the opening of a pore entirely, thereby reducing the porosity of the membrane. Intermediate blocking falls between standard and complete blocking, and is when a pore becomes only partially blocked. Finally, cake formation occurs when molecules build up on the surface of the membrane, as described previously for NFF. Models that combine these four mechanisms have also been developed to describe their interdependence on one another to elicit fouling (Ho & Zydney, A Combined Pore Blockage and Cake Filtration Model for Protein Fouling During Microfiltration, 2000; Duclos-Orsello & Ho, 2007).

It has been shown that the classical blocking models can be defined by the following equation:

$$\frac{d^2t}{dV^2} = \alpha\left(\frac{dt}{dV}\right)^{\beta} \quad (5)$$

where V is the permeate volume, t is time, and α and β are constants (Hermia, 1982). The value d^2t/dV^2 gives the resistance coefficient, which is the rate of change of the instantaneous resistance to filtration with respect to permeate volume. The value of β is used to identify the mechanism of pore blockage, and thus flux decline during filtration. A value of β equal to 1.5 shows standard pore blocking, while a value of 2 is complete blocking, and finally values of 1 and 0 define intermediate blocking and cake filtration, respectively.

For virus filtration, the most common foulants are molecules such as DNA, host cell proteins (HCP), and other protein or product aggregates. Employing a 0.1µm to 0.2µm pre-filter step prior to virus filtration can significantly decrease the amount of fouling observed in virus filtration, and greatly increase flux and capacity without decreasing the yield of the desired product (Kern & Krishnan, 2006; van Reis & Zydney, 2007).

1.4 Gigantic Magnetoresistance (GMR)

Magnetoresistance is a change in the resistivity of a material due to a magnetic field. There are two main types of magnetoresistive (MR). Anisotropic magnetoresistance (AMR) is based on the intrinsic magnetoresistance of a ferromagnetic material. It is the change in material resistance when the magnetization changes from parallel, with respect to the direction of current flow, to transverse. Gigantic magnetoresistance (GMR) and spin valve sensors, on the other hand, are based on ferromagnetic/non-magnetic multilayers (Freitas, Ferreira, Cardoso, & Cardoso, 2007). Applying a magnetic field to the varying magnetic layers causes a change in the relative orientation of their magnetization. When the magnetic layers have parallel magnetization directions, spin-up electrons will be weakly scattered and spin-down electrons will be strongly scattered leading to a low electrical resistance. On the contrary, when the magnetization is antiparallel, the resistance is high due to the scattering of spin-up and spin-down electrons alternating between strong and weak. The sensors detect the change in electrical resistance in the presence of a magnetic field with a fixed current. GMR sensors are most commonly used for data storage in such

applications as read heads for a hard disk drive, magnetic random access memory (MRAM), and magnetic recording media (Graham, Ferreira, & Freitas, 2004).

GMR sensors have been identified for use in novel detection systems involving magnetic labeling of biomolecules (Freitas, Ferreira, Cardoso, & Cardoso, 2007; Graham, Ferreira, & Freitas, 2004; Li, Sun, Wilson, White, Pourmand, & Wang, 2006; Baselt, Lee, Natesan, Metzger, Sheehan, & Colton, 1998; Graham D. L., Ferreira, Freitas, & Cabral, 2003; Schotter, et al., A Biochip Based on Magnetoresistive Sensors, 2002; Mak, et al., 2010; Schotter, Kamp, Becker, Pühler, Reiss, & Brückl, Comparison of a prototype magnetoresistive biosensor to standard, 2004; Reiss, et al., 2005). Other methods for quantification and detection of magnetic particles and biomolecules, such as the super conducting quantum interference device (SQUID), have also been employed. The SQUID, however, requires highly qualified operators, complex and very large instrumentation, high power consumption, and has low sensitivity. MR devices have the ability to detect very weak magnetic fields (on the order of nT) at room temperature, are scalable, flexible, relatively inexpensive, portable, and have the capacity for extremely sensitive detection, down to a single molecule (Graham, Ferreira, & Freitas, 2004; Li, Sun, Wilson, White, Pourmand, & Wang, 2006).

Small, superparamagnetic nanoparticles can increase the sensitivity of these sensors, thus these particles are well suited to serve as virus surrogates for viral clearance studies. Employing a robust detection system with non-biological surrogates is key to implementing new advancements in nanotechnology into viral clearance and membrane integrity tests. Refer to Appendix II, for a description of the design, fabrication, and initial testing of a GMR sensor.

Chapter 2.

Experimental Methods (Membrane Filtration)

2.1 Introduction

Cell culture and virus propagation methods were employed to harvest mouse parvovirus stock, which was used in membrane filtration studies to mimic true biotechnology feed streams. Virus was quantified using traditional PCR methods. In the future, these filtration experiments will be repeated with virus surrogates comprised of superparamagnetic nanoparticles, and then directly compared. The virus quantification results will also be correlated to quantification of magnetic particles after filtration. The goal of this work is to provide a true, biological standard which will be used to validate magnetic nanoparticles as virus surrogates, and validate the magnetoresistive device as a sensitive, robust detection method for surrogates in membrane applications.

2.2 Cell Culture

A9 mouse (*Mus musculus*) fibroblast cells (ATCC #CCL-1.4, Manassas, VA) were used in these experiments (Littlefield, 1963). A frozen cryovial containing A9 cells from ATCC was rapidly thawed in a water bath at 37°C. After thawing, the cells were added to a 15ml conical tube containing 10ml of fresh culture medium. Standard culture medium for A9 cells consists of high glucose (4.5 g/L) Dulbecco's Minimal Essential Medium (DMEM) containing L-glutamine (Hyclone, Logan, UT) supplemented with 10% heat inactivated fetal bovine serum (FBS, Hyclone, Logan, UT). The contents were centrifuged at 1000 RPM for 5 minutes, the supernatant was discarded, and 10ml of fresh medium was added to the pellet. The resuspended cells were transferred to a $25cm^2$ cell culture filter flask and incubated at 37°C and 10% CO_2. Cells were observed daily using an inverted microscope until they reached greater than 90% confluence, typically within 2-3 days.

Upon reaching confluence, the cell culture medium was discarded from the vessel, and cells were rinsed with 5ml Dulbecco's phosphate buffered saline (DPBS) solution, pH 7.4 (Invitrogen, Carlsbad, CA). The DPBS was discarded and 1.5ml of 0.05% trypsin, 0.53 mM EDTA (Invitrogen, Carlsbad, CA) was added to the vessel. The vessel was rocked at room temperature until cells began to round up as observed by the

inverted microscope, approximately 60 seconds. Next, 1ml of trypsin-EDTA was removed, leaving 0.5ml in the vessel. The vessel was rocked every 30 seconds until the cells began to visibly detach. Cells were rinsed from the bottom of the flask by aspirating 5ml of fresh culture medium over the detaching monolayer. The suspension was aspirated several times to dispense the cells and they were transferred to a 15ml conical tube. 100µl of the suspension was removed in order to determine the cell density by staining with 0.4% Trypan blue dye (Hyclone, Logan, UT). The cells were counted using a hemacytometer. A cell concentration of 5×10^6 cells was used to start a new culture in a $75cm^2$ cell culture filter flask or 1×10^7 cells for a $150cm^2$ cell culture filter flask. Cells were incubated, observed for confluence, and expanded into multiple vessels using the method for detachment described previously, except increasing reagent volume proportionally to the vessel size.

2.3 Virus Propagation

One culture vessel was trypsinized as described previously to obtain a cell count using the Trypan blue staining method, also described previously. The cell count was used to determine the amount of virus to dilute in 1ml of culture media to achieve a multiplicity of infection (MOI) of 0.001. Stock aliquots of Minute Virus of Mice (MVM) (ATCC # VR-1346) were obtained from -80°C storage, and thawed rapidly in a water bath at 37°C. The media was discarded from all cell culture vessels, and each flask was inoculated with 1ml of pre-diluted virus (per $75cm^2$ cell culture filter flask). The vessels were incubated at 37°C and 10% CO_2 for 90 minutes, with gentle rocking approximately every 10 minutes. After the 90 minute adsorption, the vessel was rinsed with 3ml of DPBS and 20ml of fresh culture media was added. The vessels were incubated at 37°C and 10% CO_2 and monitored daily with an inverted microscope for cytopathic effects (CPE) and pH. pH was buffered by adding small drops of 7.5% sodium bicarbonate solution (Invitrogen, Carlsbad, CA) to medium until it remained orange to red in color. Virus infected media was harvested at the height of CPE, typically 10 days after infection. Culture medium was frozen and thawed three times by freezing in the -80°C freezer and rapidly thawing in a 37°C water bath. Medium was placed in 50ml centrifuge tubes and centrifuged at 5000 RPM for 5 minutes to remove cell debris. Virus stock was stored at -80°C.

2.4 Filtrate

Frozen MVM stock virus was thawed rapidly in a 37°C water bath, and spiked into a solution of high glucose DMEM containing L-glutamine (Hyclone, Logan, UT) to a concentration of 10^8 virus particles/ml. These solutions are referred to as low protein solutions. In order to determine the effect of high protein loads in the feed stream, bovine serum albumin (BSA) (Sigma-Aldrich, St. Louis, MO) was suspended in phosphate buffered saline (PBS) pH 7.4 to a concentration of 1% (w/v). 1% (w/v) BSA in 1X PBS pH 7.0 – 7.4 is the recommended protein, concentration, and pH for small virus retention experiments (Brorson, et al., 2008). MVM stock virus was spiked into the solution to a concentration of 10^8 virus particles/ml. These solutions are referred to as high protein solutions. The high protein solution was sterile filtered through a 0.2µm sterile filter unit (Nalgene, Rochester, NY) to remove large protein aggregates.

2.5 Filtration

Filtration experiments were conducted using feed streams consisting of low protein and high protein solutions containing 10^8 virus particles/ml as described previously. The solution was filtered in a standard 200ml, model 8200 Amicon stirred cell (Millipore, Billerica, MA) in normal (dead-end) filtration mode at a constant pressure of 30psi (0.2 MPa) in a biological safety cabinet. Figure 1 is a schematic representation of the filtration set up. Table 2 summarizes the various membranes tested. All membranes were single sheets, placed with the filtration surface away from the feed stream for the asymmetric membranes, and with a non-woven support underneath to prevent damage to the membrane from the stirred cell (Freudenberg and Co., Weinheim, Germany), seen previously (Bakhshayeshi & Zydney, 2008; Bohonak & Zydney, 2005; Syedain, Bohonak, & Zydney, 2006). Membranes were cut into 42 mm disks from large flat sheets using a specially designed cutting device. Approximately 500µl sample aliquots, for virus and protein analysis, were taken from the filtrate stream for every 10ml of permeate collected. First, pure water permeance was measured, followed by flux during virus filtration, and DI water flux of the fouled membrane. Flux was recorded using a top loading balance to weigh permeate and recorded on Balance link Software from Mettler Toledo.

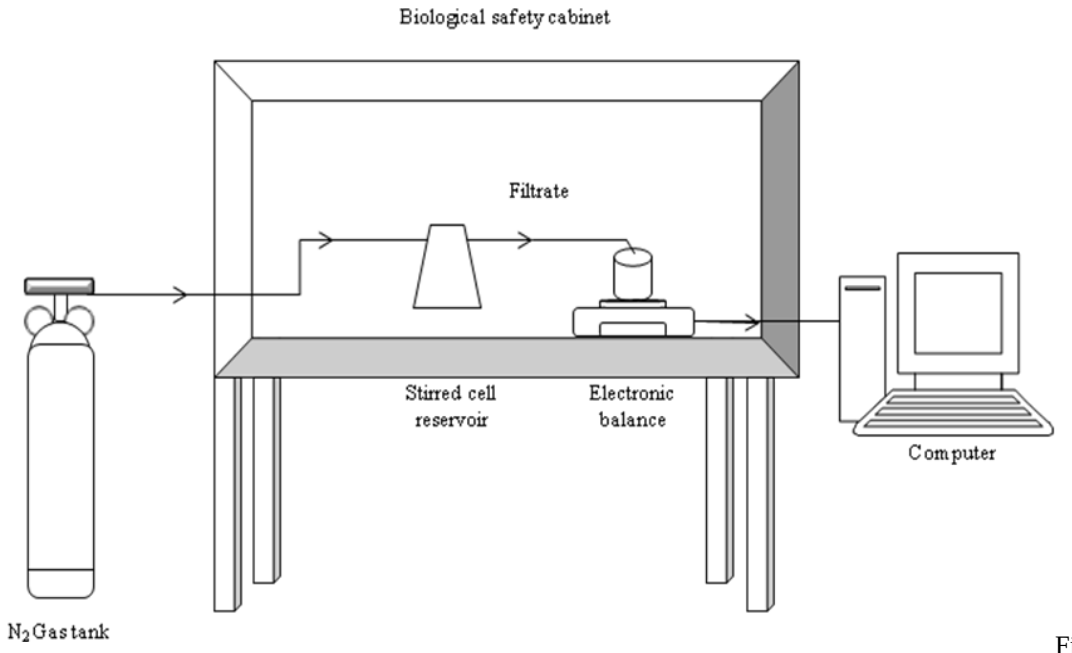

Figure 2. Experimental Setup

Table 2. Membranes (Pall Corporation, 2009; Millipore, 2009)

Trade Name	Manufacturer	Membrane	Commercial Application and Comments
Ultipor VF grade DV 20	Pall	Hydrophilic modified polyvinylidene fluoride	Normal flow virus filtration membrane used as a double layer ≥3 log reduction for viruses > 20 nm ≥6 log reduction for virus > 50 nm Operating pressure of 0.1 – 0.3 MPa
Omega 300		Modified polyethersulfone	Tangential flow ultrafiltration membrane 300kDa nominal molecular weight cut off Maximum operating pressure of 0.4 MPa
Omega 10		Modified polyethersulfone	Tangential flow ultrafiltration membrane 10kDa nominal molecular weight cut off Maximum operating pressure of 0.4 MPa
RVRM	Millipore	Polyethersulfone	Normal flow virus filtration membrane used as a triple layer ≥6 log reduction for virus > 80 nm Approximate maximum operating pressure of 0.35 MPa
Viresolve® Pro (VP)		Hydrophilic polyethersulfone	Normal flow virus filtration membrane used as a double layer with corresponding device ≥4 log reduction for viruses > 20 nm Approximate maximum operating pressure of 0.35 MPa
Biomax 10 PBGC		Modified polyethersulfone	Tangential flow or normal flow ultrafiltration membrane 10kDa nominal molecular weight cut off Approximate maximum operating

			pressure of 0.4 MPa

2.6 Virus Quantification

Virus concentration in cell culture media and for all experimental results was determined by real time polymerase chain reaction (RT-PCR). 9µl of DNase master mix [water, DNase buffer (400mM Tris-HCl, 100mM $MgSO_4$, and 10mM $CaCl_2$), and RQ1 DNase (Promega, Madison, WI)] was aliquoted to each well of a 96-well plate for each sample that required testing. This DNase treatment was included in order to eliminate any naked DNA in the sample. Each sample was tested in duplicate. 1µl of sample was added to each well containing DNase master mix and the plate was covered. The plate was spun in a centrifuge until the velocity reached approximately 800 RPM, then immediately stopped. The plate was incubated in a 37°C water bath for 40 minutes. SYBR green master mix (containing dNTPs, 50U/ml iTaq DNA polymerase, 6 mM $MgCl_2$, SYBR Green I, and 20nM fluorescein) (BioRad, Hercules, CA), forward primer (GAC GCA CAG AAA GAG AGT AAC CAA), and reverse primer (CCA ACC ATC TGC TCC AGT AAA CAT) (Ros, Burckhardt, & Kempf, 2002) were thawed rapidly by hand. The PCR master mix was prepared in a microcentrifuge tube by adding 10µl SYBR green master mix, 8.2µl water, 0.4µl (100 nM) forward primer, and 0.4µl (100 nM) reverse primer to the tube for every reaction. 19µl of PCR master mix was added to each well in a fresh 96 well plate, and 1µl of DNase treated sample was added to the PCR master mix. Eight standards, ranging from 10^2 copies/µl to 10^9 copies/µl, were thawed and included with each plate. The standards were created previously by cloning the 501 base pair PCR product (from the full MVM genome) into a pCR 2.1 cloning plasmid (TOPO® Clone, Invitrogen, Carlsbad, CA). Plasmids were grown on standard bacterial culture, followed by the use of QIAGEN plasmid Maxi preparation kit (QIAGEN, Valencia, CA). The final product yielded a volume of 1ml at a concentration of 2.1µg/µl. The final product was diluted to 1 x 10^9 copies per µl and standards created by further serial diluting to 1 x 10^0 copies per ul. Standards were stored frozen at -20°C. The plate was analyzed in a Bio-Rad iCycler iQ5 RT-PCR machine. The protocol consists of a 10 minute, 95°C initial DNase heat inactivation step, which also denatures MVM virus particles to expose genomic DNA. The following cycle parameters were repeated 45 times: Denaturation step - 95°C, 10 seconds; Annealing step - 57°C, 15 seconds; Elongation step - 72°C 30 seconds; Final step - 72°C, 10 seconds with real-time data collection. The limit of detection of this assay was determined previously by analyzing each standard (down to 1 x 10^0 copies per µl) in

triplicate on a single plate. Statistical Probit analysis (using Minitab) was used to plot the confidence of detection and the limit of detection was determined at 95% confidence to be 13.7 copies/µl. For the purposes of the experiments conducted here, 10^8 particles/ml of virus are added to feed streams. Since the lowest, detectable amount of virus is 1.37×10^4 particles/ml, the limit of detection is a virus reduction of 4 logs.

2.7 Bovine Serum Albumin (BSA) Assay

Protein concentration was measured using a BCA Protein Assay Kit (Pierce, Rockford, IL) following manufacturer's instructions. Using a 96 well microplate (Nalge Nunc International, Rochester, NY), 25µl of unknown sample or standard albumin was added to the wells. 200µl of working reagent was added to each well. The plate was covered and incubated at 37°C for 30 minutes. After cooling to room temperature, the absorbance of each sample at 562nm was measured using a Benchmark Plus Microplate Spectrophotometer (Bio-Rad). As described by the manufacturer, the protein concentration was determined and reported with reference to a standard albumin solution provided by the manufacturer. All samples were analyzed in triplicate and average results are reported. For feed streams spiked with 1% (w/v) BSA, the majority of protein present was BSA.

2.8 Critical Point Drying for Scanning Electron Microscopy

To prevent pore collapse, critical point drying was performed prior to analyzing samples with a JEOL field emission scanning electron microscope (JSM-6500F, JEOL Ltd., Tokyo, Japan). Small membrane samples were placed into specimen holder baskets. Baskets were placed directly into the liquid transfer boat filled with absolute ethanol, and then into the critical point drying apparatus. Cold tap water was run to the jacket of the chamber, after which the chamber was filled with liquid carbon dioxide and allowed to sit for 5-10 minutes. With the vent valve slightly open to maintain the carbon dioxide liquid level, the drain valve was opened to remove the absolute ethanol for approximately 3-5 minutes. The flushing action was repeated approximately 7 times, until the absolute ethanol had been completed substituted. After flushing was complete, liquid carbon dioxide again filled the chamber. The cold water was substituted for hot tap water until the temperature of the chamber reached approximately 36-38°C. The carbon dioxide gas that formed

was then slowly vented off. Samples were removed from the chamber and the baskets, and mounted to microscope stubs. Samples were then coated with 10nm of gold.

Chapter 3.

Results and Discussion

3.1 Membrane Evaluation

Figures 3 and 4 give FESEM images of the six membranes tested. All membranes, except for the DV 20, are considered asymmetric and are of a composite structure. Although the porosity of the downstream surface appears lower than that for the upstream side, the DV 20 is considered symmetric by the manufacturer. It is clear that the ultrafiltration membranes, Omega 300, Omega 10 and PBGC, have a much larger asymmetric distribution across the membrane than for the two asymmetric virus filters, RVRM and VP. The asymmetry of the virus filtration membranes allows for the more open pores structures to act as a support and an in-line prefilter to remove aggegrates prior to reaching the smaller pore surface when run with the skin side facing downstream (Syedain, Bohonak, & Zydney, 2006).

The Omega 10 has an extremely dense filtration surface that makes it difficult to visualize its porosity. Similarly, PBGC (with the same MWCO of 10kDa as Omega 10) has a very dense skin surface, which may have experienced some cracking emanating at the very small pores during the critical point drying procedure. The Omega 300, on the other hand, is easily visualized as it has the largest pores as well as the broadest pore size distribution. Both the RVRM and VP virus filtration membranes have greater porosity than the DV 20, and it appears these membranes have a variable pores size distribution.

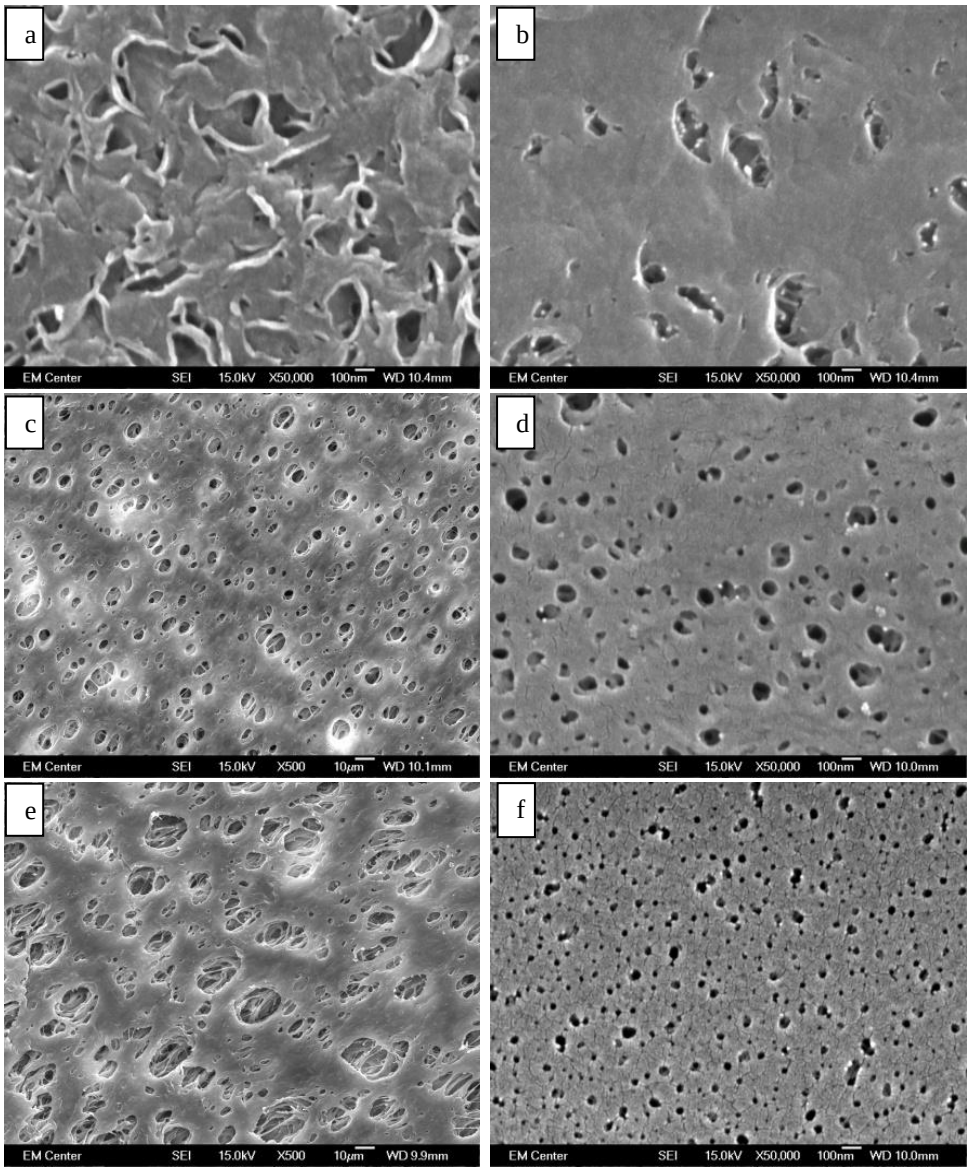

Figure 3. (Left column) FESEM images of the upstream surface of virus filtration membranes DV 20 (a), RVRM (c), and VP (e) at a magnification of 500 times, except for the DV 20 which is shown at a magnification of 50,000 times. (Right column) FESEM images of the downstream surface of DV 20 (b), RVRM (d), VP (f) at a magnification of 50,000 times.

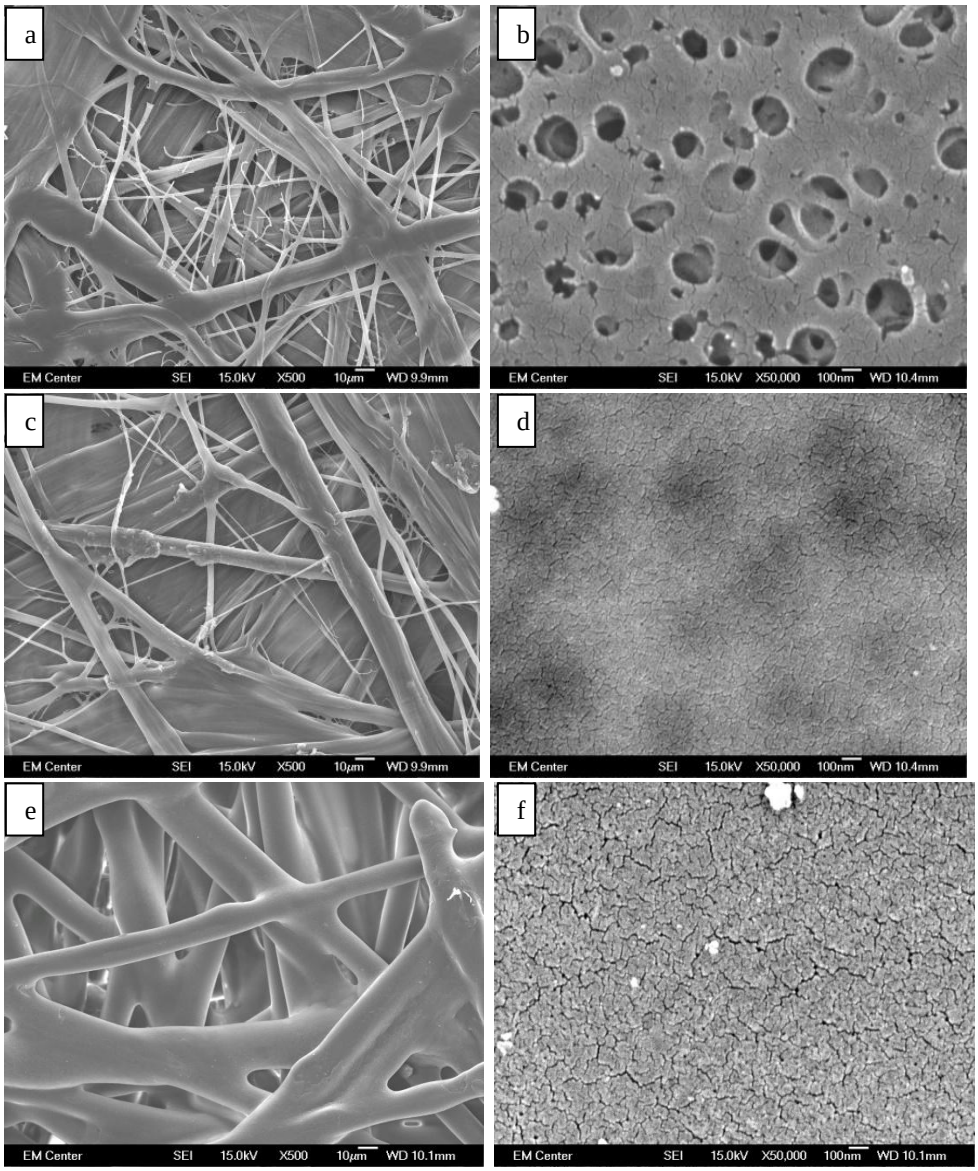

Figure 4. (Left column) FESEM images of the upstream surface of ultrafiltration membranes Omega 300 (a), Omega 10 (c), and PBGC (e) at a magnification of 500 times. (Right column) FESEM images of the downstream surface of Omega 300 (b), Omega 10 (d), and PBGC (f) at a magnification of 50,000 times.

Figure 5 provides water fluxes at 0.2MPa. All fluxes are reported as differential results. Porosity, pore size distribution, and thickness are all contributing factors to pure water flux rates. RVRM and Omega 300 appear to have similar water fluxes although the Omega 300 has a larger nominal pore size than RVRM. Millipore product information states that the permeability of the RVRM membrane is 100 L m^{-2} h^{-1} psi^{-1}, which gives a pure water flux of 3,000 L m^{-2} h^{-1} at 0.2 MPa (Millipore, 2009). Bohonak and Zydney found the permeability of PBS for the Omega 300 membrane to be 4 x 10^{-12} m at 0.1MPa (Bohonak & Zydney, 2005). Using equation (4), and accounting for experimental conditions used here, the predicted water flux would therefore be 2,880 L m^{-2} h^{-1}. The findings observed in this data are in accordance to previously predicted values.

Omega 10 and PBGC appear to have the smallest pores, but resulted in a higher water flux than DV 20 due to the low porosity of the DV 20. Pall product information predicts water fluxes of the DV 20 to be 42 L m^{-2} h^{-1} for a single layer of membrane at 0.2MPa, while Omega 10 is reported to have water flux values between 0.7-1.9 ml min^{-1} cm^{-2} at 0.37MPa (Pall Corporation, 2009). PBGC has only a slightly higher water flux than Omega 10. Under the experimental conditions used here, the estimated water flux is approximately 300 L m^{-2} h^{-1}. Again, this is in accordance with these experimental findings. The VP membrane has similar porosity to the RVRM but smaller nominal pore size altogether and it therefore falls between all other membranes.

These water flux values are important to be able to compare different filtration runs, with different membranes and feed streams to ensure operating conditions remain the same from run to run.

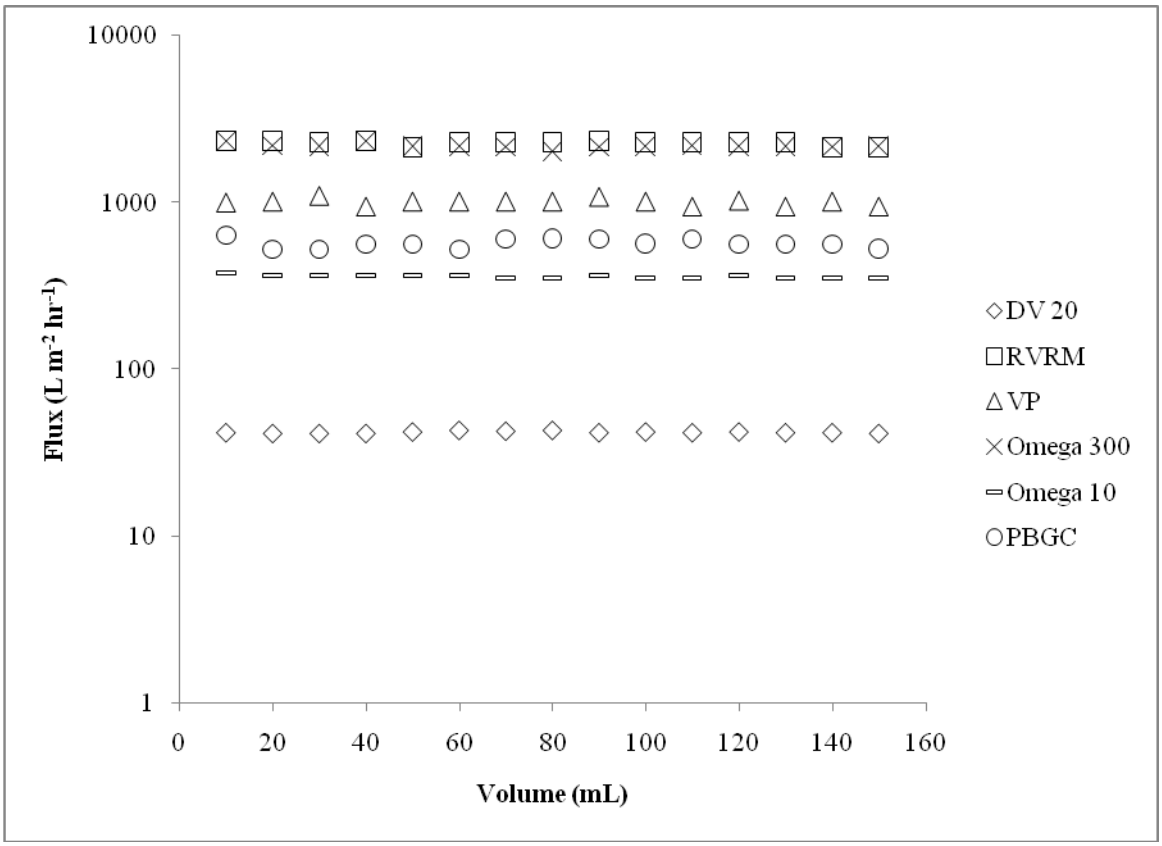

Figure 5. Pure Water Fluxes at 0.2MPa

3.2 Virus/Protein Rejection and Fouling

Figure 6 shows permeate fluxes for virus loaded feed streams that did not contain BSA. All membranes appear to have similar fluxes to that seen with the pure water experiments, except the PBGC had a very slight flux decrease. Figure 7 shows permeate fluxes for virus loaded feed streams that contained 1% (w/v) BSA. For all membranes, except RVRM, there is a decrease in permeate flux with volume processed. In the case of the Omega 10, the flux decline was so drastic that permeate was not collected after 110ml was processed. For all other membranes, 150ml of permeate was collected and analyzed. Compared to Figure 6, it is evident that flux decrease is attributed to the presence of BSA.

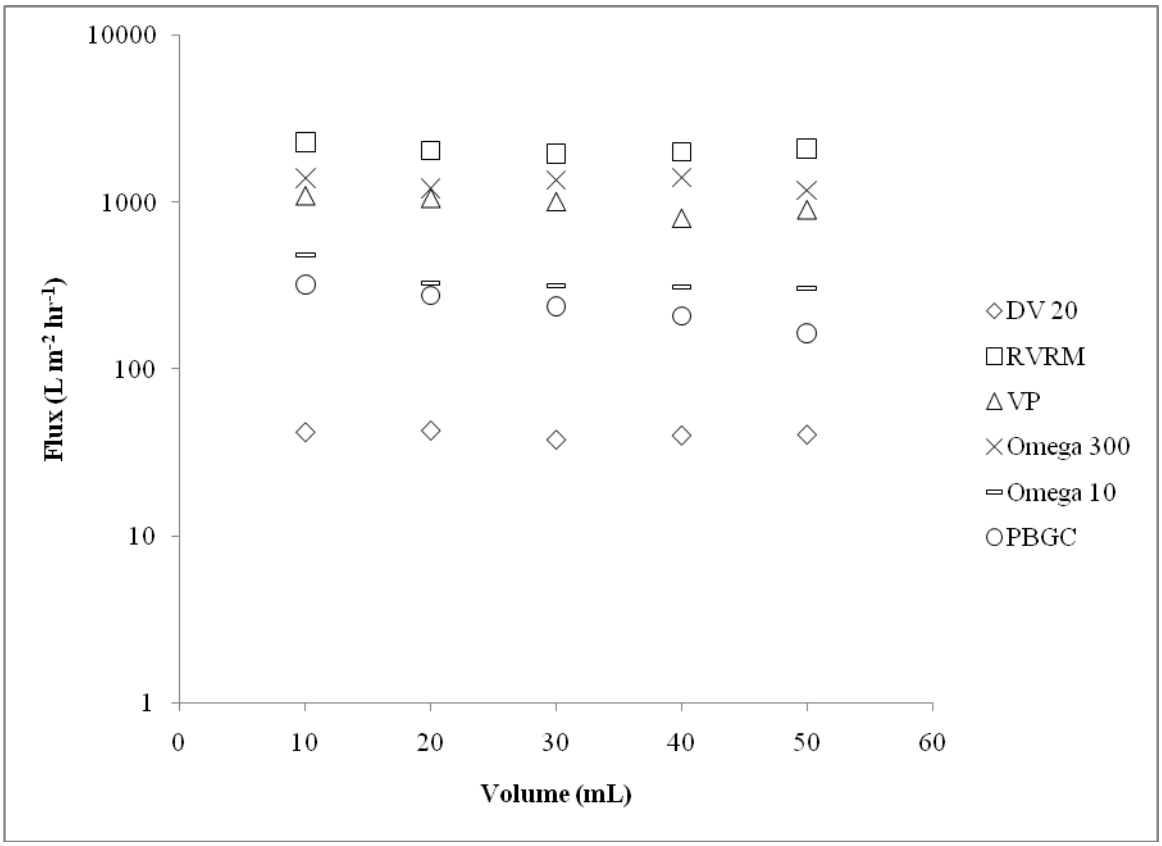

Figure 6. Fluxes Obtained for Filtration of Feed Streams Containing MVM in the Absence of Protein

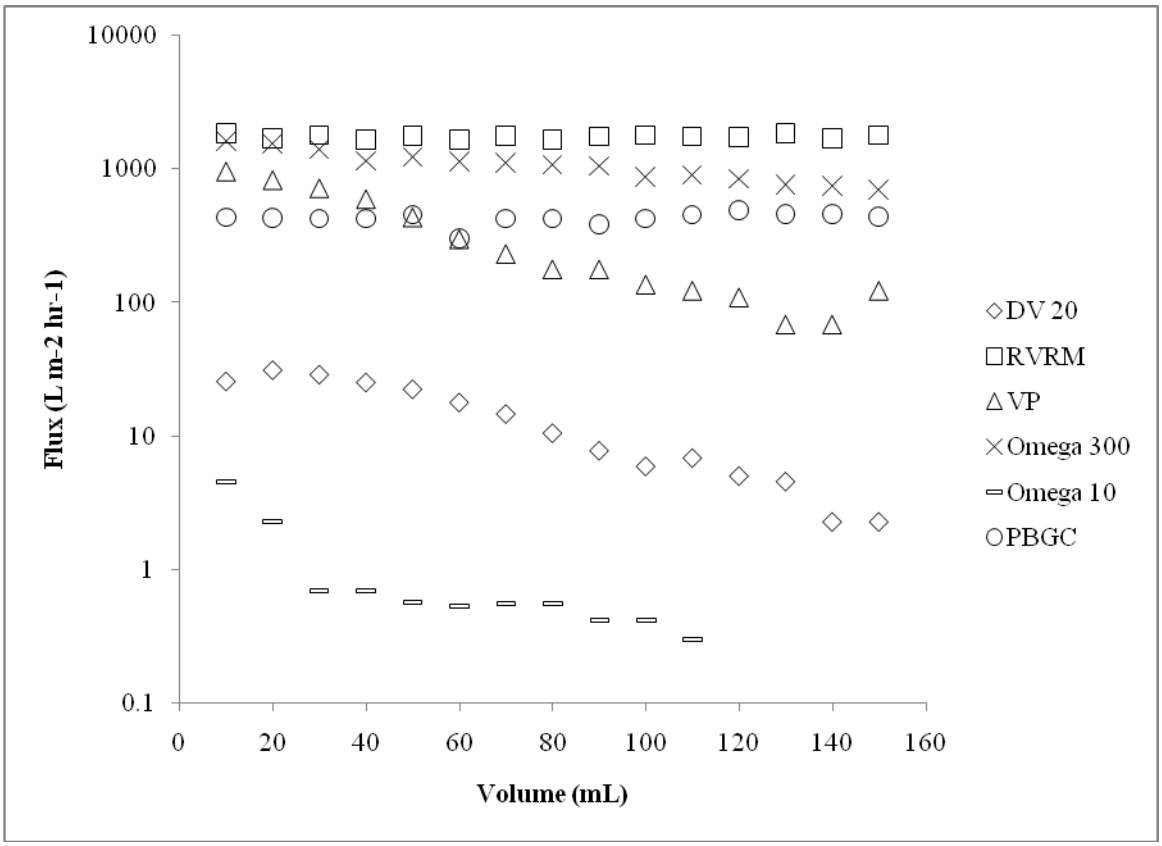

Figure 7. Fluxes Obtained for Filtration of Feed Streams Containing MVM and 1% (w/v) BSA

Figures 8 and 9 show the log reduction of virus from the feed stream to the permeate in the absence and presence of 1% (w/v) BSA, respectively. The DV 20 showed a two to four log reduction in virus regardless of the presence of BSA, which is consistent with the manufacturer's reports. It is important to note that all membranes were tested in a single layer, while the DV 20, VP, and RVRM membranes are sold commercially as multilayer devices that are likely to provide higher virus retention. PBGC and VP experienced a decrease in the rejection of virus in the presence of BSA, while rejection for the Omega 300, Omega10, and RVRM appears to have slightly increased in the presence of protein. It has been observed previously, that virus rejection can decline with extended throughputs. This has been attributed to partial or complete pore blockage of the pores on the smaller end of the distribution thereby diverting more flow to the larger pores where virus can pass (Brorson, et al., 2008).

The RVRM membrane exhibits low levels of viral clearance, as expected due to its application as a retroviral filter, with nominal pore sizes greater than 20nm. It is clear in Figure 4b that the pore sizes for the Omega 300 are much greater than those of the RVRM, so the low level of viral clearance observed for the Omega 300 is also expected. Although the VP membrane is designed to reject parvovirus, low levels of virus clearance (≤ 1 $\log_{10}$ reduction) were observed. Again, as noted previously, the DV 20, VP, and RVRM membranes are typically operated in multiple sheets, while data observed here is from single sheet experiments. Although the pore sizes and MWCO rating for the Omega 10 indicate that parvovirus would be rejected, less than 1 $\log_{10}$ rejection was observed for this membrane. Similarly, the PBGC is expected to have high parvovirus rejection, however significant decrease in rejection was observed with feed streams containing protein. Since the Omega 10 and PBGC membranes are designed to be operated with the skin surface upstream to the feed and in TFF mode, virus and protein rejections not consistent with manufacturer's reports are likely. This low rejection of virus may be caused by virus particle entrapment within fluid in the more open pore structure of the asymmetric membrane. The presence of even a few relatively large pores can result in the passage of the virus particles. This is especially true when an osmotic pressure difference is created between the high protein concentration on the membrane surface and the bulk feed. High protein concentrations become entrapped in the membrane support structure causing an internal concentration polarization.

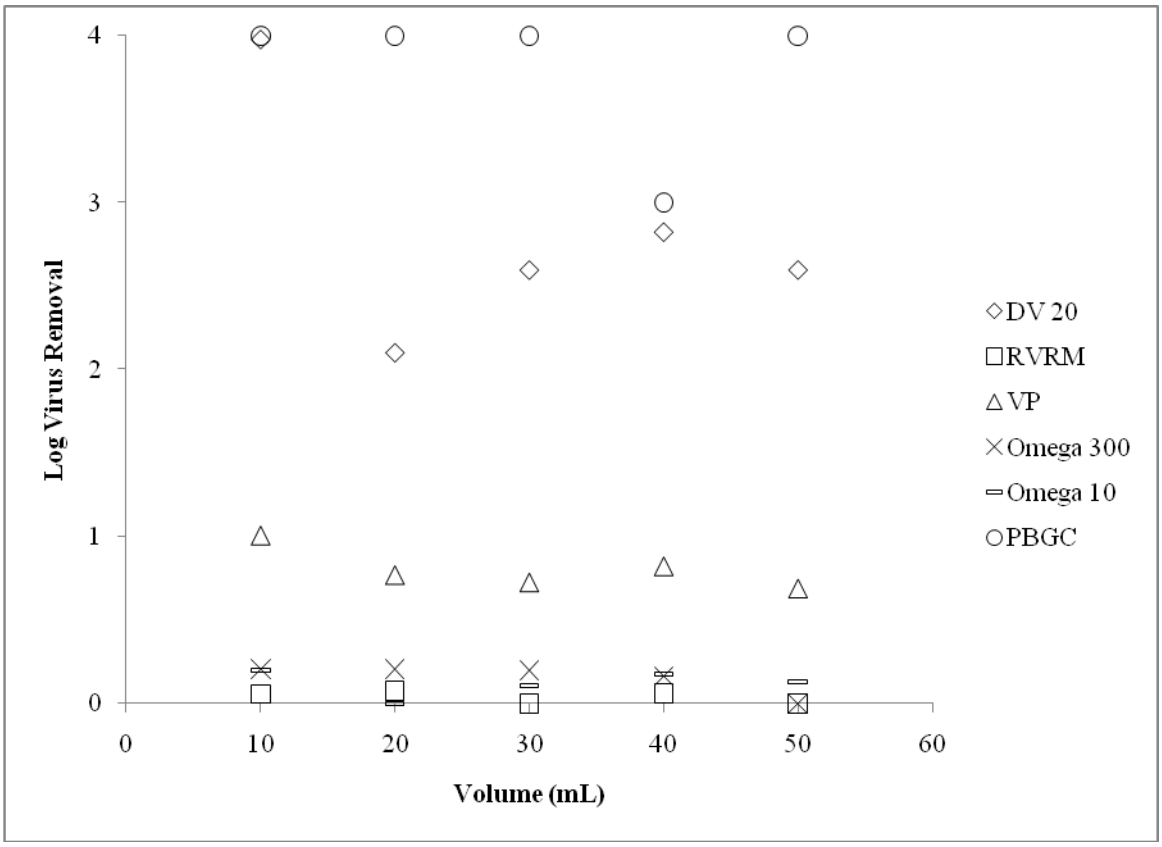

Figure 8. Log Reduction of Virus from Feed Streams Spiked with MVM not Containing Protein

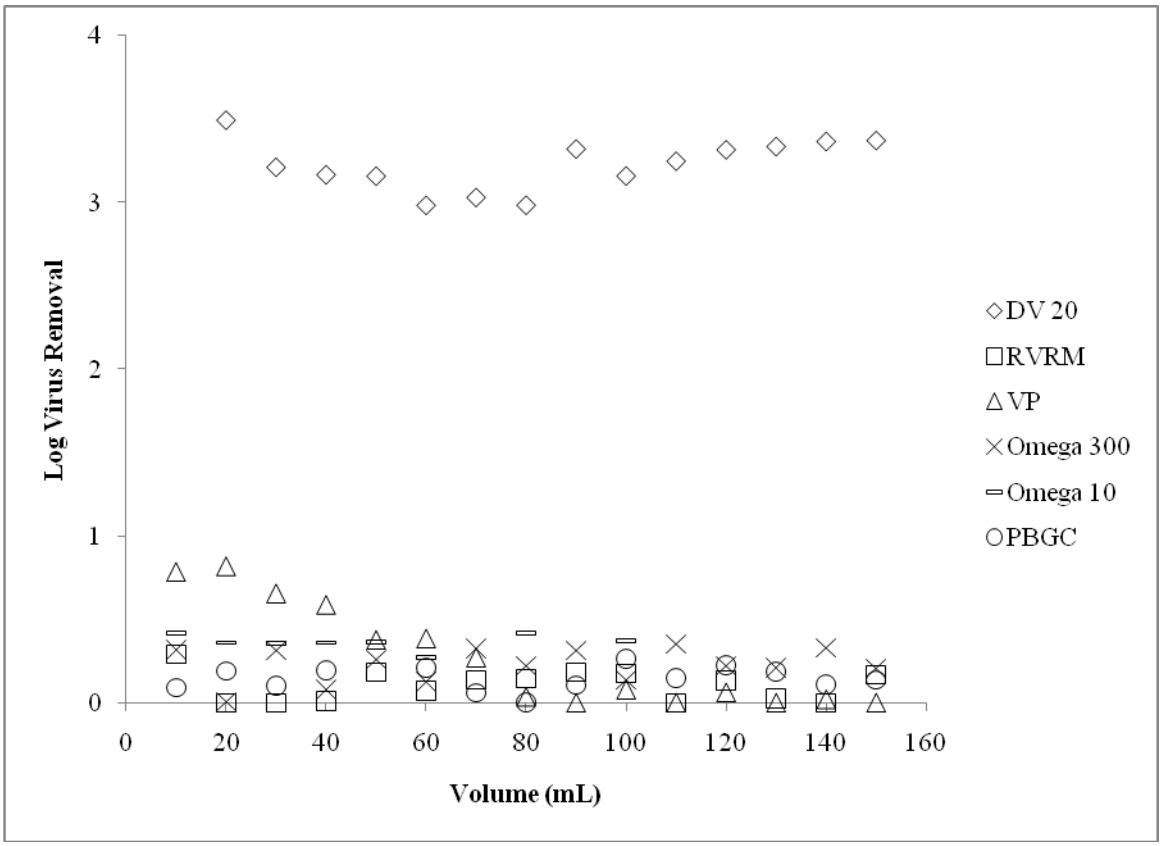

Figure 9. Log Reduction of Virus from Feed Streams Spiked with MVM and 1% (w/v) BSA

Figure 10 shows the water flux of each membrane both before filtration (as in Figure 3), as well as after virus filtration with 1% (w/v) BSA. All membranes experienced a water flux decline, except for the RVRM membrane. The Omega 300 flux prior to filtration is similar to that of the RVRM, and so is masked behind the RVRM results in the figure. Omega 10 is not included here due to the extreme flux decline observed in Figure 6, causing early termination of the filtration. The effect of the fouling deposit can be evaluated by comparing membrane resistance for the clean membrane and the fouled membrane using the following equation:

$$R_m = \frac{\Delta P}{\mu J_v} \qquad (5)$$

where ΔP is the transmembrane pressure difference, μ is the solution viscosity, and J_v is the filtrate velocity (Syedain, Bohonak, & Zydney, 2006). A significant change in resistance was observed for all membranes except RVRM, indicating that the flux decline is due to irreversible fouling. Increase in resistance is thought to be due to the deposition of the protein within the more open support structure of the membrane.

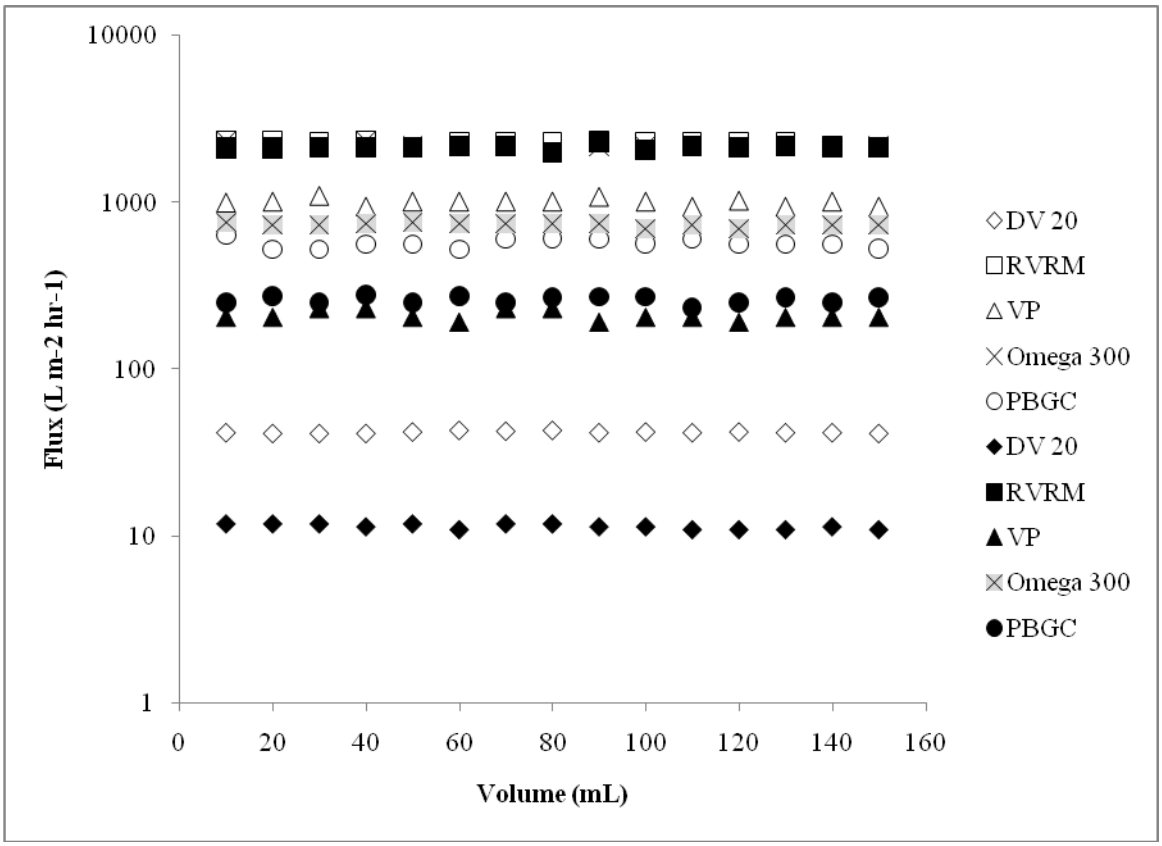

Figure 10. Comparison of Water Flux Before Filtration (open symbols) and After Filtration with 1% (w/v) BSA (filled symbols)

Table 3 shows the overall observed BSA transmission, where the overall transmission is defined as that which was observed in a sample of bulk permeate. BSA, MW 70kDa, transmission was observed with all membranes. Furthermore, BSA feed streams were pre-filtered with a 0.2µm sterile filter to remove large protein aggregates. BSA rejection was not expected for the DV 20, RVRM, Omega 300, and VP membranes as their MWCO are greater than 70kDa. Rejection of BSA was expected, however, for the Omega 10 and PBGC membranes, which have a MWCO of 10kDa (Pall Corporation, 2009; Millipore, 2009). Since the Omega 10 and PBGC showed only approximately 25 to 20% rejection, it is likely that the extreme fouling of the membrane caused blockage of all pores on the lower end of the broad pore size distribution, thus forcing both virus and protein through the larger pores, before those became fouled causing early termination of the operation. Boyd and Zydney have evaluated Omega 30 and 50 membranes in NFF mode with the filtration surface either towards or away from the feed stream. When the membranes were operated with the selective barrier facing the feed stream, dextran rejection coefficients were in agreement with the manufacturer's specifications. When the membranes were operated in the opposite mode, however, the rejection coefficients that were obtained were up to an order of magnitude less than specified by the manufacture (Boyd & Zydney, 1997). These findings are similar to the observations observed with the low BSA and virus rejection for the Omega 10 and PBGC membranes.

Table 3. Overall BSA Transmission for Feed Streams Containing MVM and 1% (w/v) BSA

Membrane	BSA Transmission Percentage
DV 20	>0.90
RVRM	>0.97
VP	>0.91
Omega 300	>0.91
Omega 10	<0.78
PBGC	<0.80

Figure 11, on the other hand, illustrates percent transmission of BSA in a feed solution containing MVM and 1% (w/v) BSA through each membrane at each permeate collection interval. Transmission at each fraction is quite variable, and is expected for those membranes with a MWCO greater than BSA (i.e., DV 20, RVRM, Omega 300, and VP membranes). Fractions experiencing greater than 100 percent transmission are in agreement with the previous observation that protein and virus within the more open

pore structure of the asymmetric membrane can get pushed through the pores on the larger end of the pore size distribution as high pressure causes flow around these interconnected pores.

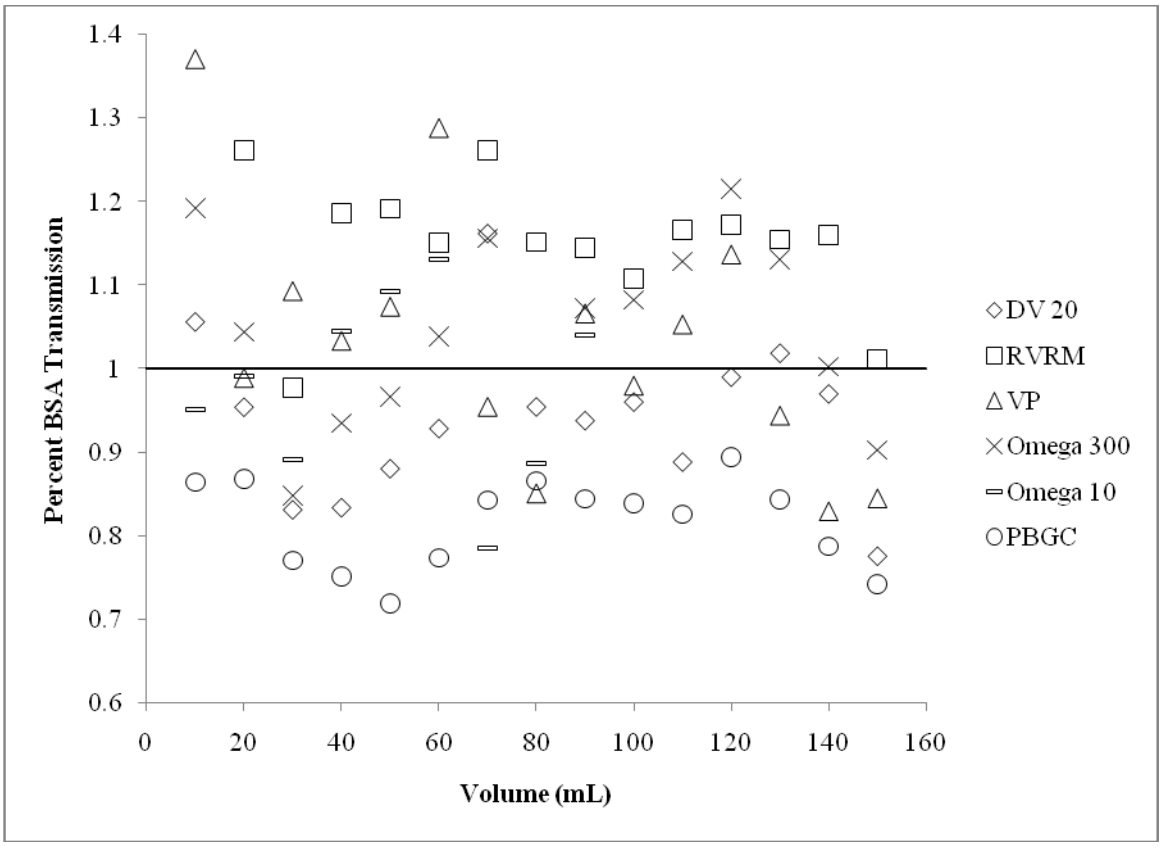

Figure 11. BSA Transmission

The BSA assay experienced a lot of variance from sample to sample, and as a result, another method of protein quantification should be used to reevaluate protein transmission through the membranes in the presence of virus or virus surrogate.

Chapter 4.

Conclusions

Viral contamination of biotechnology products is a serious concern that requires elaborate testing in order to assure safety. Virus filtration plays an important role in the removal of virus from these products. Viral clearance studies, demonstrating the removal of such contaminants, would greatly benefit from the use of a non-biological virus surrogates.

Six commercially available membranes were examined for their virus and protein filtration properties. Membranes were operated in normal flow filtration mode, where asymmetric membranes were placed with their selective barrier (skin side) facing away from the feed stream. Feed streams containing MVM as a nonspecific model virus and 1% (w/v) BSA were used to challenge membranes. The results obtained will be directly correlated to experiments conducted with super paramagnetic virus surrogates in order to ensure that such surrogates behave as real viruses in membrane filtration aspects. Employing a wide variety of membranes ensures that the viral clearance properties of the surrogates are evaluated thoroughly.

An effective virus filter rejects model viruses, while allowing the passage of greater than 98 percent of the protein or product of interest. Many factors come into play when evaluating virus filters such as porosity, pore size distribution, operating conditions, and membrane structure. Fouling of membranes is also influential in viral clearance. Size exclusion removal of viruses is based upon pore sizes that are smaller than virus (approximately 20-100nm), but larger than protein (approximately <10nm). Narrow pore size distributions are crucial for the successful filtration of viruses; however, some variations in pore size inevitably occur during membrane manufacture. As filtration progresses, the smallest pores become completely blocked by feed protein (as seen in Figure 12). The liquid flow through smaller pores decreases or stops, and fluid flow is rerouted through the large pores either directly or via pore interconnectivity, thereby allowing passage of both virus and perhaps protein. For the ultrafiltration membranes Omega 10 and PBGC tested here, however, the pore sizes are designed to retain (and eventually concentrate) protein (less than 10kDa), when operated in their typical tangential flow fashion with the selective barrier (skin

side) directly facing the feed stream. When operated in reverse (with the support structure facing the feed stream) in NFF mode, high levels of both virus and protein transmission were observed. Complete pore blockage was observed by both membranes, with severe flux decline. In contrast, virus rejection increased slightly in the presence of protein for membranes rated with larger pore sizes. Both scenarios observed here have been reported before. Decrease in virus retention and flux over time have been observed, while increased virus retention has been observed in the presence of a flocculating agent (Bolton, Cabatingan, Rubino, Lute, Brorson, & Bailey, 2005; Akeprathumchai, Han, Wickramasinghe, Carlson, Czermak, & Prei, 2004; Wickramasinghe, Han, Carlson, & Powers, 2004). These results should be mimicked by the virus surrogate in order to ensure that a surrogate will appropriately represent a true viral contamination.

Chapter 5.

Future Work

While normal flow filtration mode is less costly and more simplistic than tangential flow filtration, virus filters as well as ultrafiltration membranes were originally designed to be operated in TFF mode. Successful virus rejection has been observed by operating ultrafiltration membranes in TFF mode (DiLeo, Allegrezza, & Builder, 1992). Operating these membranes in NFF mode puts a significant amount of pressure and compaction on the membrane itself once seated in a stirred cell. Leaking of the stirred cell due to incorrect sealing can occur, although it was not physically observed here. A comparison of virus rejection and protein transmission of these six membranes operated in tangential flow filtration mode could be made with the results obtained here. Additionally, evaluating the use of multiple layers and/or filtration devices seen in industry (e.g., DV 20, VP, and RVRM membranes) under NFF and TFF mode would help to determine one mode of operation as a more reliable source of viral clearance than another.

References

Akeprathumchai, S., Han, B., Wickramasinghe, S. R., Carlson, J. O., Czermak, P., & Prei, K. (2004). Murine Leukemia Virus Clearance by Flocculation and Microfiltration. *Biotechnology and Bioengineering , 88* (7), 880-889.

Akita, G. Y., Ianconescu, M., MacLachlan, N. J., & Osburn, B. I. (1994, March 12). Bluetongue Disease in Dogs Associated with Contaminated Vaccine. *The Veterinary Record* , 283-284.

Aranha-Creado, H., & Brandwein, H. (1999). Application of Bacteriophages as Surrogates for Mammalian Viruses: A Case for Use in Filter Validation Based on Precedents and Current Practices in Medical and Environmental Virology. *Journal of Pharmaceutical Science and Technology , 53* (2), 75-82.

ATCC. (2010). *VR-1346™ Product Description*. Retrieved March 2010, from American Type Culture Collection: http://www.atcc.org/ATCCAdvancedCatalogSearch/ProductDetails/tabid/452/Default.aspx?ATCCNum=VR-1346&Template=animalVirology

Bakhshayeshi, M., & Zydney, A. L. (2008). Effect of Solution pH on Protein Transmission and Membrane Capacity During Virus Filtration. *Biotechnology and Bioengineering , 100* (108-117).

Baselt, D. R., Lee, G. U., Natesan, M., Metzger, S. W., Sheehan, P. E., & Colton, R. J. (1998). A biosensor based on magnetoresistance technology. *Biosensors and Bioelectronics , 13*, 731–739.

Bohonak, D. M., & Zydney, A. L. (2005). Compaction and Permeability Effects with Virus Filtration Membranes. *Journal of Membrane Science , 254*, 71-79.

Bolton, G., Cabatingan, M., Rubino, M., Lute, S., Brorson, K., & Bailey, M. (2005). Normal-flow Virus Filtration: Detection and Assessment of the Endpoint in Bioprocessing. *Biotechnol. Appl. Biochem. , 42*, 133-142.

Boschetti, N., Niederhauser, I., Kempf, C., Stühler, A., Löwer, J., & Blümel, J. (2004). Different susceptibility of B19 virus and mice minute virus to. *Transfusion , 44* (7), 1079-1086 .

Boschetti, N., Wyss, K., Mischler, A., Hostettler, T., & Kempf, C. (2003). Stability of minute virus of mice against temperature and. *Biologicals , 31*, 181-185.

Boyd, R. F., & Zydney, A. L. (1997). Sieving Characteristics of Multilayer Ultrafiltration Membranes. *Journal of Membrane Science , 131*, 155-165.

Brorson, K., Campbell, J., Carter, J., Dolan, S., Krishnan, M., Lute, S., et al. (2008). Virus Filtration Technical Report No. 41. *Supplement to the PDA Journal of Pharmaceutical Science and Technology , 62* (S-4), 1-62.

Brough, H., Antoniou, C., Carter, J., Jakubik, J., Xu, Y., & Lutz, H. (2002). Performance of a Novel Viresolve NFR Virus Filter. *Biotechnology Progress , 18*, 782-795.

Burstyn, D. (1996). Contamination of Genetically Engineered Chinese Hamster Ovary Cells. *Developments in Biological Standardization , 88*, 199-203.

Carbone, M., Rizzo, P., & Pass, H. I. (1997). Simian virus 40, poliovaccines and human tumors: a review of recent developments. *Oncogene , 15*, 1877-1888.

Deluhery, J., & Rajagopalan, N. (2008). Use of Paramagnetic Particles in Membrane Integrity Testing. *Journal of Membrane Science , 318*, 176-181.

DiLeo, A. J., Allegrezza, A. E., & Builder, S. E. (1992). High Resolution Removal of Virus from Protein Solutions Using a Membrane of Unique Structure. *Bio/Technology , 10*, 182-188.

Duclos-Orsello, C., & Ho, C. C. (2007). Letter to the Editor: Comment on the Combined Pore Blockage and Pore Constriction Model. *Journal of Membrane Science , 297*, 297.

Erickson, G. A., Bolin, S. R., & Lundgraf, J. G. (1991). Viral contamination of fetal bovine serum used for tissue culture: risks and concerns. *Developments in Biological Standardization , 75*, 173-175.

Eterpi, M., McDonnell, G., & Thomas, V. (2009). Disinfection efficacy against parvoviruses. *Journal of Hospital Infection , 73*, 64-70.

FDA. (1998, September 24). Guidance on Viral Safety Evaluation of Biotechnology Products Derived from Cell Lines of Human or Animal Origin. *Federal Register , 63 , 185*. Food and Drug Administration, Department of Health and Human Services.

FDA/CBER. (1993). Points to Consider in the Characterization of Cell Lines Used to Produce Biologicals. Rockville, MD: Food and Drug Administration, Center for Biologics Evaluation and Research.

FDA/CBER. (1997). Points to Consider in the Manufacture and Testing of Monoclonal Antibody Products for Human Use. Rockville, MD: Food and Drug Administration/Center for Biologics Evaluation and Research.

Fox, J. P., Manso, C., Penna, H. A., & Para, M. (1942). Observations on the Occurrence of Icterus in Brazil Following Vaccination Against Yellow Fever. *American Journal of Hygiene , 36* (1), 68-116.

Freitas, P. P., Ferreira, R., Cardoso, S., & Cardoso, F. (2007). Magnetoresistive sensors. *Journal of Physics: Condensed Matter , 19* (165221), 1-21.

Furuya, K., Murai, K., Yokoyama, T., Maeno, H., Takeda, Y., Murozuka, T., et al. (2006). Implementation of a 20-nm pore-size filter in the plasmaderived. *Vox Sanguinis , 91*, 119-125.

Garnick, R. L. (1996). Experience with viral contamination in cell culture. *Developments in Biological Standardization , 88*, 49-56.

Genzyme Corporation. (2009, June 16). *Genzyme Temporarily Interrupts Production at Allston Plant*. Retrieved December 20, 2009, from http://www.genzyme.com/corp/media/GENZ%20PR-061609.asp

Graham, D. L., Ferreira, H. A., & Freitas, P. P. (2004). Magnetoresistive-based biosensors and biochips. *TRENDS in Biotechnology , 22* (9), 455-462.

Graham, D. L., Ferreira, H. A., Freitas, P. P., & Cabral, J. M. (2003). High sensitivity detection of molecular recognition using magnetically. *Biosensors and Bioelectronics , 18*, 483 - 488.

Harasawa, R. (1995). Adventitious pestivirus RNA in live virus vaccines against bovine and swine diseases. *Vaccine , 13* (1), 100-103.

Harasawa, R., & Sasaki, T. (1995). Sequence Analysis of the 5' Untranslated Region of Pestivirus RNA Demonstrated in Interferons for Human Use. *Biologicals , 23*, 263-269.

Harasawa, R., & Tomiyama, T. (1994). Evidence of Pestivirus RNA in Human Virus Vaccines. *Journal of Clinical Microbiology , 32* (6), 1604-1605.

Harris, R. J., Dougherty, R. M., Biggs, P. M., Payne, L. N., Goffe, A. P., Churchill, A. E., et al. (1966). Contaminant Viruses in Two Live Virus Vaccines Produced in Chick Cells. *The Journal of Hygiene (Cambridge) , 64* (1), 1-7.

Hermia, J. (1982). Constant Pressure Blocking Filtration Law - Applications to Power-law Non-Newtonian Fluids. *Transactions of the Institution of Chemical Engineers , 60*, 183-187.

Ho, C. C., & Zydney, A. L. (2000). A Combined Pore Blockage and Cake Filtration Model for Protein Fouling During Microfiltration. *Journal of Colloid and Interface Science , 232* (2), 389-399.

Ho, C. C., & Zydney, A. L. (2002). Transmembrane Pressure Profiles During Constant Flux Microfiltration of Bovine Serum Albumin. *Journal of Membrane Science , 209*, 363-377.

ICH. (2008). *The International Conference on Harmonisation of Technical Requirements for Registration of Pharmaceuticals for Human Use*. Retrieved October 10, 2008, from http://www.ich.org

Kern, G., & Krishnan, M. (2006). Virus Removal by Filtration: Points to Consider. *BioPharm International , 19* (10).

Kulkarni, S. S., Funk, W. E., & Li, N. N. (2001). Ultrafiltration. In W. S. Ho, & K. K. Sirkar (Eds.), *Membrane Handbook* (pp. 391-453). Norwell: Kluwer Academic Publishers.

Li, G., Sun, S., Wilson, R. J., White, R. L., Pourmand, N., & Wang, S. X. (2006). Spin Valve Sensors for Ultrasensitive Detection of Superparamagnetic Nanoparticles for Biological Applications. *Sensors and Actuators A , 126*, 98-106.

Littlefield, J. W. (1963). The Inosinic Acid Pyrophosphorylase Activity of Mouse Fibroblasts Partially Resistant to 8-. *Proceedings of the National Academy of Sciences of the United States of America , 50* (3), 568-576.

Loh, S., Beuscher, U., Poddar, T. K., Porter, A. G., Wingard, J. M., Husson, S. M., et al. (2009). Interplay Among Membrane Properties, Protein Properties, and Operating Conditions on Protein Fouling During Normal-Flow Microfiltration. *Journal of Membrane Science , 332*, 93-103.

Mak, A. C., Osterfeld, S. J., Yu, H., Wang, S. X., Davis, R. W., Jejelowo, O. A., et al. (2010). Sensitive giant magnetoresistive-based immunoassay for multiplex. *Biosensors and Bioelectronics , 25*, 1635–1639.

Merten, O. W. (2002). Virus contamination of cell cultures - A biotechnological view. *Cytotechnology , 39*, 91-116.

Millipore. (2009). Billerica, MA.

Minor, P. (1996). Mammalian Cells and Their Contaminants. *Developments in Biological Standardization , 88*, 25-29.

Moore, W. A. (1992). Experience in Cell Line Testing. *Developments in Biological Standardization , 76*, 51-56.

Nettleton, P. F., & Rweyemamu, M. M. (1980). The Association of Calf Serum with the Contamination of BHK 21 Clone 12 Suspension Cells by a Parvovirus Serologically Related to the Minute Virus of Mice (MVM). *Archives of Virology , 64*, 359-374.

Nims, R. (2009, December 18). Viral Contamination of Biologics. Longmont, CO, USA.

Nims, R. W. (2006). Detection of Adventitious Viruses in Biologicals - A Rare Occurence. (J. a. Petricciani, Ed.) *Dev. Biologicals , 123*, 153-164.

Nims, R. W., Dusing, S. K., Hsieh, W. T., Lovatt, A., Reid, G. G., Onions, D., et al. (2008). Detection of Cache Valley Virus in Biologics Manufactured in CHO Cells. *Biopharm International , 21*, 89-94.

Oehmig, A., Buttner, M., Weiland, F., Werz, W., Bergemann, K., & Pfaff, E. (2003). Identification of a calcivirus isolate of unknown origin. *Journal of General Virology , 84*, 2837-2845.

Pall Corporation. (2009). Port Washington, NY.

Rabenau, H., Ohlinger, V., Anderson, J., Selb, B., Cinatl, J., Wolf, W., et al. (1993). Contamination of genetically engineered CHO-cells by epizootic haemorrhagic disease virus (EHDV). *Biologicals , 21*, 207-214.

Reiss, G., Brueckl, H., Huetten, A., Schotter, J., Brzeska, M., Panhorst, M., et al. (2005). Magnetoresistive sensors and magnetic nanoparticles for biotechnology. *Journal of the Materials Research Society , 20* (12), 3294-3302.

Ros, C., Burckhardt, C. J., & Kempf, C. (2002). Cytoplasmic Trafficking of Minute Virus of Mice: Low-pH Requirement, Routing to Late Endosomes, and Proteasome Interaction. *Journal of Virology , 76* (24), 12634-12645.

Schotter, J., Kamp, P. B., Becker, A., Pühler, A., Brinkmann, D., Schepper, W., et al. (2002). A Biochip Based on Magnetoresistive Sensors. *IEEE Transactions on Magnetics , 38* (5), 3365-3367.

Schotter, J., Kamp, P. B., Becker, A., Pühler, A., Reiss, G., & Brückl, H. (2004). Comparison of a prototype magnetoresistive biosensor to standard. *Biosensors and Bioelectronics , 19*, 1149–1156.

Shah, K., & Nathanson, N. (1976). Human exposure to SV40: review and comment. *American Journal of Epidemiology , 103*, 1-12.

Strauss, J. H., & Strauss, E. G. (2002). *Viruses and Human Disease.* San Diego: Academic Press.

Susanto, H., & Ulbricht, M. (2008). Polymeric Membranes for Molecular Separation. In E. Drioli, & L. Giorno (Eds.), *Membrane Operations: Innovative Separations and Transformations* (pp. 1-30). VCH, Weinheim: Wiley.

Sweet, B. H., & Hilleman, M. R. (1960). The Vacuolating Virus, SV40. *Proceedings of the Society for Experimental Biology and Medicine , 105* (2), 420-427.

Syedain, Z. H., Bohonak, D. M., & Zydney, A. L. (2006). Protein Fouling of Virus Filtration Membranes: Effects of Membrane Orientation and Operating Conditions. *Biotechnology Progress , 22*, 1163-1169.

Ulbricht, M. (2006). Advanced Functional Polymer Membranes. *Polymer , 47*, 2217-2262.

van Reis, R., & Zydney, A. (2007). Biprocess Membrane Technology. *Journal of Membrane Science , 297*, 16-50.

van Voorthuizen, E. M., Ashbolt, N. J., & Schäfer, A. I. (2001). Role of Hydrophobic and ElectrostaticIinteractions for Initial Enteric Virus Retention by MF Membranes. *Journal of Membrane Science , 194*, 69-79.

Vannier, P., Leforban, Y., Carnero, R., & Cariolet, R. (1988). Contamination of a Live Virus Vaccine Against Psuedorabies (Aujeszky's Disease) by an Ovine Pestivirus Pathogen for the Pig. *Ann Rech Vet , 19*, 283-290.

Wickramasinghe, S. R. (2008). Tangential Flow Filtration for Virus Capture. In N. N. Li, A. G. Fane, W. S. Ho, & T. Matsuura (Eds.), *Advanced Membrane Technology and Applications.* Hoboken: Wiley.

Wickramasinghe, S. R., Han, B., Carlson, J. O., & Powers, S. M. (2004). Clearance of Minute Virus of Mice by Flocculation and Microfiltration. *Biotechnology and Bioengineering , 86* (6), 612-621.

Appendix I: Real Time PCR Data

Feed Streams Spiked with MVM not Containing Protein:

Well	Fluor	Type	Identifier	Replicate #	Starting Quantity (SQ)	Log Starting Quantity	SQ Mean	SQ Std. Dev.
A02	SYBR	Unkn	DV-20 10ml	39	0	0	0	0
B02	SYBR	Unkn	DV-20 10ml	39	1.475E+08	8.169	1.48E+08	0.00E+00
C02	SYBR	Unkn	DV-20 20ml	2	0	0	0	0
D02	SYBR	Unkn	DV-20 20ml	2	2.157E+08	8.334	2.16E+08	0.00E+00
E02	SYBR	Unkn	DV-20 30ml	3	1.781E+08	8.251	1.62E+08	2.25E+07
F02	SYBR	Unkn	DV-20 30ml	3	1.464E+08	8.165	1.62E+08	2.25E+07
G02	SYBR	Unkn	DV-20 40ml	4	0	0	0	0
H02	SYBR	Unkn	DV-20 40ml	4	0	0	0	0
A03	SYBR	Unkn	DV-20 50ml	5	3.971E+07	7.599	1.15E+08	1.07E+08
B03	SYBR	Unkn	DV-20 50ml	5	1.912E+08	8.282	1.15E+08	1.07E+08
C03	SYBR	Unkn	DV-20 Total	6	0	0	0	0
D03	SYBR	Unkn	DV-20 Total	6	0	0	0	0
C11	SYBR	Unkn	Negative Control	38	0	0	0	0
D11	SYBR	Unkn	Negative Control	38	1.840E+09	9.265	1.84E+09	0.00E+00
A05	SYBR	Unkn	OT010 10ml	13	0	0	0	0
B05	SYBR	Unkn	OT010 10ml	13	0	0	0	0
C05	SYBR	Unkn	OT010 20ml	14	0	0	0	0
D05	SYBR	Unkn	OT010 20ml	14	0	0	0	0
E05	SYBR	Unkn	OT010 30ml	15	3.379E+07	7.529	2.15E+07	1.74E+07
F05	SYBR	Unkn	OT010 30ml	15	9.155E+06	6.962	2.15E+07	1.74E+07
G05	SYBR	Unkn	OT010 40ml	16	0	0	0	0
H05	SYBR	Unkn	OT010 40ml	16	0	0	0	0
A06	SYBR	Unkn	OT010 50ml	17	0	0	0	0

B06	SYBR	Unkn	OT010 50ml	17	0	0	0	0
C06	SYBR	Unkn	OT010 Total	18	0	0	0	0
D06	SYBR	Unkn	OT010 Total	18	0	0	0	0
E03	SYBR	Unkn	OT300 10ml	7	0	0	0	0
F03	SYBR	Unkn	OT300 10ml	7	0	0	0	0
G03	SYBR	Unkn	OT300 20ml	8	0	0	0	0
H03	SYBR	Unkn	OT300 20ml	8	0	0	0	0
A04	SYBR	Unkn	OT300 30ml	9	0	0	0	0
B04	SYBR	Unkn	OT300 30ml	9	0	0	0	0
C04	SYBR	Unkn	OT300 40ml	10	0	0	0	0
D04	SYBR	Unkn	OT300 40ml	10	0	0	0	0
E04	SYBR	Unkn	OT300 50ml	11	0	0	0	0
F04	SYBR	Unkn	OT300 50ml	11	0	0	0	0
G04	SYBR	Unkn	OT300 Total	12	8.648E+09	9.937	8.63E+09	1.92E+07
H04	SYBR	Unkn	OT300 Total	12	8.620E+09	9.936	8.63E+09	1.92E+07
E06	SYBR	Unkn	PBGC 10ml	19	1.921E+07	7.284	1.92E+07	0.00E+00
F06	SYBR	Unkn	PBGC 10ml	19	0	0	0	0
G06	SYBR	Unkn	PBGC 20ml	20	3.534E+07	7.548	3.53E+07	0.00E+00
H06	SYBR	Unkn	PBGC 20ml	20	0	0	0	0
A07	SYBR	Unkn	PBGC 30ml	21	5.238E+07	7.719	5.24E+07	0.00E+00
B07	SYBR	Unkn	PBGC 30ml	21	0	0	0	0
C07	SYBR	Unkn	PBGC 40ml	22	3.652E+07	7.562	3.65E+07	0.00E+00
D07	SYBR	Unkn	PBGC 40ml	22	0	0	0	0
E07	SYBR	Unkn	PBGC 50ml	23	0	0	0	0
F07	SYBR	Unkn	PBGC 50ml	23	0	0	0	0
G07	SYBR	Unkn	PBGC Total	24	1.756E+07	7.245	9.93E+06	1.08E+07
H07	SYBR	Unkn	PBGC Total	24	2.306E+06	6.363	9.93E+06	1.08E+07

A11	SYBR	Unkn	Positive control	37	9.759E+08	8.989	2.36E+09	1.95E+09
B11	SYBR	Unkn	Positive control	37	3.736E+09	9.572	2.36E+09	1.95E+09
E09	SYBR	Unkn	RVRM 10ml	31	0	0	0	0
F09	SYBR	Unkn	RVRM 10ml	31	0	0	0	0
G09	SYBR	Unkn	RVRM 20ml	32	9.781E+04	4.990	9.78E+04	0.00E+00
H09	SYBR	Unkn	RVRM 20ml	32	0	0	0	0
A10	SYBR	Unkn	RVRM 30ml	33	1.156E+10	10.063	5.91E+09	7.99E+09
B10	SYBR	Unkn	RVRM 30ml	33	2.538E+08	8.404	5.91E+09	7.99E+09
C10	SYBR	Unkn	RVRM 40ml	34	1.424E+09	9.153	1.42E+09	0.00E+00
D10	SYBR	Unkn	RVRM 40ml	34	0	0	0	0
E10	SYBR	Unkn	RVRM 50ml	35	6.324E+07	7.801	6.32E+07	0.00E+00
F10	SYBR	Unkn	RVRM 50ml	35	0	0	0	0
G10	SYBR	Unkn	RVRM Total	36	0	0	0	0
H10	SYBR	Unkn	RVRM Total	36	2.721E+09	9.435	2.72E+09	0.00E+00
A01	SYBR	Std	Standard 1	1	1.000E+02	2.000	0.00E+00	0.00E+00
B01	SYBR	Std	Standard 2	2	1.000E+03	3.000	0.00E+00	0.00E+00
C01	SYBR	Std	Standard 3	3	1.000E+04	4.000	1.00E+04	0.00E+00
D01	SYBR	Std	Standard 4	4	1.000E+05	5.000	0.00E+00	0.00E+00
E01	SYBR	Std	Standard 5	5	1.000E+06	6.000	1.00E+06	0.00E+00
F01	SYBR	Std	Standard 6	6	1.000E+07	7.000	1.00E+07	0.00E+00
G01	SYBR	Std	Standard 7	7	1.000E+08	8.000	1.00E+08	0.00E+00
H01	SYBR	Std	Standard 8	8	1.000E+09	9.000	1.00E+09	0.00E+00
A08	SYBR	Unkn	VP 10ml	25	1.128E+08	8.052	1.13E+08	0.00E+00
B08	SYBR	Unkn	VP 10ml	25	0	0	0	0
C08	SYBR	Unkn	VP 20ml	26	0	0	0	0
D08	SYBR	Unkn	VP 20ml	26	0	0	0	0
E08	SYBR	Unkn	VP 30ml	27	0	0	0	0
F08	SYBR	Unkn	VP 30ml	27	0	0	0	0
G08	SYBR	Unkn	VP 40ml	28	4.598E+07	7.663	4.60E+07	0.00E+00
H08	SYBR	Unkn	VP 40ml	28	0	0	0	0

A09	SYBR	Unkn	VP 50ml	29	0	0	0	0
B09	SYBR	Unkn	VP 50ml	29	0	0	0	0
C09	SYBR	Unkn	VP Total	30	0	0	0	0
D09	SYBR	Unkn	VP Total	30	0	0	0	0

Feed Streams Spiked with MVM and 1% BSA (w/v):

Well	Fluor	Type	Identifier	Replicate #	Starting Quantity (SQ)	Log Starting Quantity	SQ Mean	SQ Std. Dev.
G11	SYBR	Unkn	Blank	39	0	0	0	0
G12	SYBR	Unkn	Blank	39	0	0	0	0
A03	SYBR	Unkn	Omega 10K – 10	1	1.908E+04	4.281	1.91E+04	4.17E+01
A04	SYBR	Unkn	Omega 10K – 10	1	1.902E+04	4.279	1.91E+04	4.17E+01
H03	SYBR	Unkn	Omega 10K – 100	8	2.022E+04	4.306	2.13E+04	1.57E+03
H04	SYBR	Unkn	Omega 10K – 100	8	2.245E+04	4.351	2.13E+04	1.57E+03
B03	SYBR	Unkn	Omega 10K – 20	2	2.122E+04	4.327	2.18E+04	8.38E+02
B04	SYBR	Unkn	Omega 10K – 20	2	2.241E+04	4.350	2.18E+04	8.38E+02
C03	SYBR	Unkn	Omega 10K – 30	3	1.890E+04	4.276	2.21E+04	4.59E+03
C04	SYBR	Unkn	Omega 10K – 30	3	2.540E+04	4.405	2.21E+04	4.59E+03
D03	SYBR	Unkn	Omega 10K – 40	4	1.793E+04	4.254	2.22E+04	6.11E+03
D04	SYBR	Unkn	Omega 10K – 40	4	2.657E+04	4.424	2.22E+04	6.11E+03
E03	SYBR	Unkn	Omega 10K – 50	5	1.807E+04	4.257	2.20E+04	5.55E+03
E04	SYBR	Unkn	Omega 10K – 50	5	2.591E+04	4.414	2.20E+04	5.55E+03
F03	SYBR	Unkn	Omega 10K – 60	6	2.463E+04	4.392	2.70E+04	3.36E+03
F04	SYBR	Unkn	Omega 10K – 60	6	2.938E+04	4.468	2.70E+04	3.36E+03
G03	SYBR	Unkn	Omega 10K – 80	7	1.655E+04	4.219	1.92E+04	3.76E+03
G04	SYBR	Unkn	Omega 10K – 80	7	2.186E+04	4.340	1.92E+04	3.76E+03
B11	SYBR	Unkn	PBGC 1 - 110	34	3.273E+04	4.515	3.53E+04	3.69E+03
B12	SYBR	Unkn	PBGC 1 - 110	34	3.795E+04	4.579	3.53E+04	3.69E+03
C11	SYBR	Unkn	PBGC 1 - 120	35	2.576E+04	4.411	2.99E+04	5.83E+03
C12	SYBR	Unkn	PBGC 1 - 120	35	3.401E+04	4.532	2.99E+04	5.83E+03

D11	SYBR	Unkn	PBGC 1 - 130	36	3.478E+04	4.541	3.24E+04	3.42E+03
D12	SYBR	Unkn	PBGC 1 - 130	36	2.995E+04	4.476	3.24E+04	3.42E+03
B09	SYBR	Unkn	PBGC 1 - 30	26	3.070E+04	4.487	4.06E+04	1.40E+04
B10	SYBR	Unkn	PBGC 1 - 30	26	5.048E+04	4.703	4.06E+04	1.40E+04
C09	SYBR	Unkn	PBGC 1 - 40	27	3.408E+04	4.532	3.18E+04	3.17E+03
C10	SYBR	Unkn	PBGC 1 - 40	27	2.960E+04	4.471	3.18E+04	3.17E+03
D09	SYBR	Unkn	PBGC 1 - 50	28	3.307E+04	4.519	7.41E+04	5.80E+04
D10	SYBR	Unkn	PBGC 1 - 50	28	1.150E+05	5.061	7.41E+04	5.80E+04
E09	SYBR	Unkn	PBGC 1 - 60	29	2.788E+04	4.445	3.07E+04	4.03E+03
E10	SYBR	Unkn	PBGC 1 - 60	29	3.358E+04	4.526	3.07E+04	4.03E+03
F09	SYBR	Unkn	PBGC 1 - 70	30	3.625E+04	4.559	4.43E+04	1.13E+04
F10	SYBR	Unkn	PBGC 1 - 70	30	5.226E+04	4.718	4.43E+04	1.13E+04
G09	SYBR	Unkn	PBGC 1 - 80	31	4.105E+04	4.613	5.08E+04	1.38E+04
G10	SYBR	Unkn	PBGC 1 - 80	31	6.051E+04	4.782	5.08E+04	1.38E+04
H09	SYBR	Unkn	PBGC 1 - 90	32	3.285E+04	4.517	3.97E+04	9.68E+03
H10	SYBR	Unkn	PBGC 1 - 90	32	4.653E+04	4.668	3.97E+04	9.68E+03
H07	SYBR	Unkn	PBGC 1 – 10	24	3.850E+04	4.585	4.04E+04	2.62E+03
H08	SYBR	Unkn	PBGC 1 – 10	24	4.220E+04	4.625	4.04E+04	2.62E+03
A11	SYBR	Unkn	PBGC 1 – 100	33	2.934E+04	4.467	2.71E+04	3.18E+03
A12	SYBR	Unkn	PBGC 1 – 100	33	2.484E+04	4.395	2.71E+04	3.18E+03
E11	SYBR	Unkn	PBGC 1 – 140	37	3.786E+04	4.578	3.87E+04	1.24E+03
E12	SYBR	Unkn	PBGC 1 – 140	37	3.961E+04	4.598	3.87E+04	1.24E+03
F11	SYBR	Unkn	PBGC 1 – 150	38	3.307E+04	4.519	3.66E+04	4.99E+03
F12	SYBR	Unkn	PBGC 1 – 150	38	4.013E+04	4.603	3.66E+04	4.99E+03
A09	SYBR	Unkn	PBGC 1 – 20	25	2.989E+04	4.475	3.22E+04	3.24E+03
A10	SYBR	Unkn	PBGC 1 – 20	25	3.447E+04	4.537	3.22E+04	3.24E+03
A05	SYBR	Unkn	RVRM – 10	9	1.948E+04	4.289	2.64E+04	9.80E+03
A06	SYBR	Unkn	RVRM – 10	9	3.333E+04	4.523	2.64E+04	9.80E+03
B07	SYBR	Unkn	RVRM – 100	18	3.386E+04	4.530	3.31E+04	1.13E+03
B08	SYBR	Unkn	RVRM – 100	18	3.226E+04	4.509	3.31E+04	1.13E+03
C07	SYBR	Unkn	RVRM – 110	19	5.072E+04	4.705	5.36E+04	4.13E+03
C08	SYBR	Unkn	RVRM – 110	19	5.657E+04	4.753	5.36E+04	4.13E+03
D07	SYBR	Unkn	RVRM – 120	20	2.948E+04	4.470	3.76E+04	1.15E+04
D08	SYBR	Unkn	RVRM – 120	20	4.581E+04	4.661	3.76E+04	1.15E+04
E07	SYBR	Unkn	RVRM – 130	21	4.150E+04	4.618	4.76E+04	8.58E+03
E08	SYBR	Unkn	RVRM – 130	21	5.364E+04	4.729	4.76E+04	8.58E+03
F07	SYBR	Unkn	RVRM – 140	22	3.807E+04	4.581	5.24E+04	2.03E+04
F08	SYBR	Unkn	RVRM – 140	22	6.683E+04	4.825	5.24E+04	2.03E+04
G07	SYBR	Unkn	RVRM – 150	23	3.062E+04	4.486	3.42E+04	5.04E+03
G08	SYBR	Unkn	RVRM – 150	23	3.776E+04	4.577	3.42E+04	5.04E+03
B05	SYBR	Unkn	RVRM – 20	10	4.238E+04	4.627	5.39E+04	1.63E+04

B06	SYBR	Unkn	RVRM – 20	10	6.537E+04	4.815	5.39E+04	1.63E+04
C05	SYBR	Unkn	RVRM – 30	11	4.414E+04	4.645	5.21E+04	1.13E+04
C06	SYBR	Unkn	RVRM – 30	11	6.006E+04	4.779	5.21E+04	1.13E+04
D05	SYBR	Unkn	RVRM – 40	12	4.102E+04	4.613	4.97E+04	1.22E+04
D06	SYBR	Unkn	RVRM – 40	12	5.833E+04	4.766	4.97E+04	1.22E+04
E05	SYBR	Unkn	RVRM – 50	13	3.657E+04	4.563	3.27E+04	5.46E+03
E06	SYBR	Unkn	RVRM – 50	13	2.885E+04	4.460	3.27E+04	5.46E+03
F05	SYBR	Unkn	RVRM – 60	14	4.176E+04	4.621	4.22E+04	6.58E+02
F06	SYBR	Unkn	RVRM – 60	14	4.269E+04	4.630	4.22E+04	6.58E+02
G05	SYBR	Unkn	RVRM – 70	15	3.061E+04	4.486	3.70E+04	9.06E+03
G06	SYBR	Unkn	RVRM – 70	15	4.343E+04	4.638	3.70E+04	9.06E+03
H05	SYBR	Unkn	RVRM – 80	16	3.112E+04	4.493	3.62E+04	7.15E+03
H06	SYBR	Unkn	RVRM – 80	16	4.124E+04	4.615	3.62E+04	7.15E+03
A07	SYBR	Unkn	RVRM – 90	17	2.996E+04	4.477	3.26E+04	3.71E+03
A08	SYBR	Unkn	RVRM – 90	17	3.520E+04	4.547	3.26E+04	3.71E+03
A01	SYBR	Std	Standard 1	1	1.000E+02	2.000	1.00E+02	0.00E+00
A02	SYBR	Std	Standard 1	9	1.000E+02	2.000	1.00E+02	0.00E+00
B01	SYBR	Std	Standard 2	2	1.000E+03	3.000	1.00E+03	0.00E+00
B02	SYBR	Std	Standard 2	10	1.000E+03	3.000	1.00E+03	0.00E+00
C01	SYBR	Std	Standard 3	3	1.000E+04	4.000	1.00E+04	0.00E+00
C02	SYBR	Std	Standard 3	11	1.000E+04	4.000	1.00E+04	0.00E+00
D01	SYBR	Std	Standard 4	4	1.000E+05	5.000	1.00E+05	0.00E+00
D02	SYBR	Std	Standard 4	12	1.000E+05	5.000	1.00E+05	0.00E+00
E01	SYBR	Std	Standard 5	5	1.000E+06	6.000	1.00E+06	0.00E+00
E02	SYBR	Std	Standard 6	13	1.000E+06	6.000	1.00E+06	0.00E+00
F01	SYBR	Std	Standard 6	6	1.000E+07	7.000	1.00E+07	0.00E+00
F02	SYBR	Std	Standard 6	14	1.000E+07	7.000	1.00E+07	0.00E+00
G01	SYBR	Std	Standard 7	7	1.000E+08	8.000	1.00E+08	0.00E+00
G02	SYBR	Std	Standard 7	15	1.000E+08	8.000	1.00E+08	0.00E+00
H01	SYBR	Std	Standard 8	8	1.000E+09	9.000	1.00E+09	0.00E+00
H02	SYBR	Std	Standard 8	16	1.000E+09	9.000	0.00E+00	0.00E+00
H11	SYBR	Unkn	Stock 12/04/08	40	4.117E+04	4.615	5.11E+04	1.40E+04
H12	SYBR	Unkn	Stock 12/04/08	40	6.102E+04	4.785	5.11E+04	1.40E+04

Feed Streams Spiked with MVM and 1% BSA (w/v), continued:

Well	Fluor	Type	Identifier	Replicate #	Starting Quantity (SQ)	Log Starting Quantity	SQ Mean	SQ Std. Dev.
A03	SYBR	Unkn	DV-20 - 10	1	8.545E+00	0.932	7.82E+00	1.03E+00
A04	SYBR	Unkn	DV-20 - 10	1	7.090E+00	0.851	7.82E+00	1.03E+00

C05	SYBR	Unkn	DV-20 - 110	11	8.208E+02	2.914	8.34E+02	1.88E+01
C06	SYBR	Unkn	DV-20 - 110	11	8.474E+02	2.928	8.34E+02	1.88E+01
D05	SYBR	Unkn	DV-20 - 120	12	5.731E+02	2.758	6.09E+02	5.05E+01
D06	SYBR	Unkn	DV-20 - 120	12	6.445E+02	2.809	6.09E+02	5.05E+01
E05	SYBR	Unkn	DV-20 - 130	13	4.297E+02	2.633	5.75E+02	2.05E+02
E06	SYBR	Unkn	DV-20 - 130	13	7.198E+02	2.857	5.75E+02	2.05E+02
F05	SYBR	Unkn	DV-20 - 140	14	4.089E+02	2.612	4.90E+02	1.14E+02
F06	SYBR	Unkn	DV-20 - 140	14	5.701E+02	2.756	4.90E+02	1.14E+02
G05	SYBR	Unkn	DV-20 - 150	15	4.477E+02	2.651	4.71E+02	3.24E+01
G06	SYBR	Unkn	DV-20 - 150	15	4.935E+02	2.693	4.71E+02	3.24E+01
B03	SYBR	Unkn	DV-20 - 20	2	2.327E+02	2.367	2.70E+02	5.31E+01
B04	SYBR	Unkn	DV-20 - 20	2	3.078E+02	2.488	2.70E+02	5.31E+01
C03	SYBR	Unkn	DV-20 - 30	3	8.112E+02	2.909	1.01E+03	2.77E+02
C04	SYBR	Unkn	DV-20 - 30	3	1.203E+03	3.080	1.01E+03	2.77E+02
D03	SYBR	Unkn	DV-20 - 40	4	8.480E+02	2.928	1.30E+03	6.33E+02
D04	SYBR	Unkn	DV-20 - 40	4	1.744E+03	3.241	1.30E+03	6.33E+02
E03	SYBR	Unkn	DV-20 - 50	5	1.549E+03	3.190	1.29E+03	3.67E+02
E04	SYBR	Unkn	DV-20 - 50	5	1.030E+03	3.013	1.29E+03	3.67E+02
F03	SYBR	Unkn	DV-20 - 60	6	2.164E+03	3.335	2.95E+03	1.11E+03
F04	SYBR	Unkn	DV-20 - 60	6	3.730E+03	3.572	2.95E+03	1.11E+03
G03	SYBR	Unkn	DV-20 - 70	7	1.895E+03	3.278	2.32E+03	6.07E+02
G04	SYBR	Unkn	DV-20 - 70	7	2.753E+03	3.440	2.32E+03	6.07E+02
H03	SYBR	Unkn	DV-20 - 80	8	2.551E+03	3.407	2.85E+03	4.18E+02
H04	SYBR	Unkn	DV-20 - 80	8	3.143E+03	3.497	2.85E+03	4.18E+02
A05	SYBR	Unkn	DV-20 - 90	9	6.110E+02	2.786	5.95E+02	2.26E+01
A06	SYBR	Unkn	DV-20 - 90	9	5.791E+02	2.763	5.95E+02	2.26E+01
B05	SYBR	Unkn	DV-20 -100	10	2.127E+03	3.328	1.44E+03	9.78E+02
B06	SYBR	Unkn	DV-20 -100	10	7.445E+02	2.872	1.44E+03	9.78E+02
H09	SYBR	Unkn	Omega 300VR - 20	32	6.173E+04	4.791	5.04E+04	1.60E+04
H10	SYBR	Unkn	Omega 300VR - 20	32	3.909E+04	4.592	5.04E+04	1.60E+04
A11	SYBR	Unkn	Omega 300VR - 30	33	1.831E+04	4.263	2.52E+04	9.71E+03
A12	SYBR	Unkn	Omega 300VR - 30	33	3.204E+04	4.506	2.52E+04	9.71E+03
G09	SYBR	Unkn	Omega 300VR - 10	31	2.145E+04	4.331	2.40E+04	3.63E+03
G10	SYBR	Unkn	Omega 300VR - 10	31	2.658E+04	4.424	2.40E+04	3.63E+03
H11	SYBR	Unkn	Omega 300VR - 100	40	4.111E+04	4.614	3.68E+04	6.08E+03
H12	SYBR	Unkn	Omega 300VR – 100	40	3.251E+04	4.512	3.68E+04	6.08E+03

B11	SYBR	Unkn	Omega 300VR - 40	34	3.945E+04	4.596	4.18E+04	3.35E+03
B12	SYBR	Unkn	Omega 300VR - 40	34	4.418E+04	4.645	4.18E+04	3.35E+03
C11	SYBR	Unkn	Omega 300VR - 50	35	2.852E+04	4.455	2.75E+04	1.50E+03
C12	SYBR	Unkn	Omega 300VR - 50	35	2.641E+04	4.422	2.75E+04	1.50E+03
D11	SYBR	Unkn	Omega 300VR - 60	36	2.996E+04	4.477	3.84E+04	1.19E+04
D12	SYBR	Unkn	Omega 300VR - 60	36	4.680E+04	4.670	3.84E+04	1.19E+04
E11	SYBR	Unkn	Omega 300VR - 70	37	2.443E+04	4.388	2.35E+04	1.37E+03
E12	SYBR	Unkn	Omega 300VR - 70	37	2.250E+04	4.352	2.35E+04	1.37E+03
F11	SYBR	Unkn	Omega 300VR - 80	38	2.556E+04	4.408	3.02E+04	6.54E+03
F12	SYBR	Unkn	Omega 300VR - 80	38	3.481E+04	4.542	3.02E+04	6.54E+03
G11	SYBR	Unkn	Omega 300VR - 90	39	2.078E+04	4.318	2.45E+04	5.19E+03
G12	SYBR	Unkn	Omega 300VR - 90	39	2.813E+04	4.449	2.45E+04	5.19E+03
A01	SYBR	Std	Standard 1	1	1.000E+02	2.000	1.00E+02	0.00E+00
A02	SYBR	Std	Standard 1	9	1.000E+02	2.000	1.00E+02	0.00E+00
B01	SYBR	Std	Standard 2	2	1.000E+03	3.000	1.00E+03	0.00E+00
B02	SYBR	Std	Standard 2	10	1.000E+03	3.000	1.00E+03	0.00E+00
C01	SYBR	Std	Standard 3	3	1.000E+04	4.000	1.00E+04	0.00E+00
C02	SYBR	Std	Standard 3	11	1.000E+04	4.000	1.00E+04	0.00E+00
D01	SYBR	Std	Standard 4	4	1.000E+05	5.000	1.00E+05	0.00E+00
D02	SYBR	Std	Standard 4	12	1.000E+05	5.000	1.00E+05	0.00E+00
E01	SYBR	Std	Standard 5	5	1.000E+06	6.000	1.00E+06	0.00E+00
E02	SYBR	Std	Standard 5	13	1.000E+06	6.000	1.00E+06	0.00E+00
F01	SYBR	Std	Standard 6	6	1.000E+07	7.000	1.00E+07	0.00E+00
F02	SYBR	Std	Standard 6	14	1.000E+07	7.000	1.00E+07	0.00E+00
G01	SYBR	Std	Standard 7	7	1.000E+08	8.000	1.00E+08	0.00E+00
G02	SYBR	Std	Standard 7	15	1.000E+08	8.000	1.00E+08	0.00E+00
H01	SYBR	Std	Standard 8	8	1.000E+09	9.000	1.00E+09	0.00E+00
H02	SYBR	Std	Standard 8	16	1.000E+09	9.000	1.00E+09	0.00E+00
C09	SYBR	Unkn	VP - 120	27	3.972E+04	4.599	4.36E+04	5.43E+03
C10	SYBR	Unkn	VP - 120	27	4.740E+04	4.676	4.36E+04	5.43E+03
D09	SYBR	Unkn	VP - 130	28	4.734E+04	4.675	5.94E+04	1.70E+04
D10	SYBR	Unkn	VP - 130	28	7.138E+04	4.854	5.94E+04	1.70E+04
E09	SYBR	Unkn	VP - 140	29	4.175E+04	4.621	4.82E+04	9.12E+03
E10	SYBR	Unkn	VP - 140	29	5.464E+04	4.737	4.82E+04	9.12E+03
F09	SYBR	Unkn	VP - 150	30	6.001E+04	4.778	7.13E+04	1.60E+04

F10	SYBR	Unkn	VP - 150	30	8.261E+04	4.917	7.13E+04	1.60E+04
A07	SYBR	Unkn	VP - 20	17	6.077E+03	3.784	7.79E+03	2.43E+03
A08	SYBR	Unkn	VP - 20	17	9.507E+03	3.978	7.79E+03	2.43E+03
B07	SYBR	Unkn	VP - 30	18	8.429E+03	3.926	1.15E+04	4.31E+03
B08	SYBR	Unkn	VP - 30	18	1.453E+04	4.162	1.15E+04	4.31E+03
D07	SYBR	Unkn	VP - 50	20	1.359E+04	4.133	2.30E+04	1.33E+04
D08	SYBR	Unkn	VP - 50	20	3.242E+04	4.511	2.30E+04	1.33E+04
E07	SYBR	Unkn	VP - 60	21	1.836E+04	4.264	2.08E+04	3.39E+03
E08	SYBR	Unkn	VP - 60	21	2.315E+04	4.365	2.08E+04	3.39E+03
H05	SYBR	Unkn	VP - 10	16	6.708E+03	3.827	8.38E+03	2.36E+03
H06	SYBR	Unkn	VP - 10	16	1.005E+04	4.002	8.38E+03	2.36E+03
A09	SYBR	Unkn	VP - 100	25	3.134E+04	4.496	4.36E+04	1.73E+04
A10	SYBR	Unkn	VP - 100	25	5.576E+04	4.746	4.36E+04	1.73E+04
B09	SYBR	Unkn	VP - 110	26	4.053E+04	4.608	5.12E+04	1.51E+04
B10	SYBR	Unkn	VP - 110	26	6.183E+04	4.791	5.12E+04	1.51E+04
C07	SYBR	Unkn	VP - 40	19	1.426E+04	4.154	1.30E+04	1.77E+03
C08	SYBR	Unkn	VP - 40	19	1.175E+04	4.070	1.30E+04	1.77E+03
F07	SYBR	Unkn	VP - 70	22	1.999E+04	4.301	2.80E+04	1.13E+04
F08	SYBR	Unkn	VP - 70	22	3.596E+04	4.556	2.80E+04	1.13E+04
G07	SYBR	Unkn	VP - 80	23	3.499E+04	4.544	4.79E+04	1.83E+04
G08	SYBR	Unkn	VP - 80	23	6.084E+04	4.784	4.79E+04	1.83E+04
H07	SYBR	Unkn	VP - 90	24	4.752E+04	4.677	5.39E+04	9.09E+03
H08	SYBR	Unkn	VP - 90	24	6.037E+04	4.781	5.39E+04	9.09E+03

Feed Streams Spiked with MVM and 1% BSA (w/v), continued:

Well	Fluor	Type	Identifier	Replicate #	Starting Quantity (SQ)	Log Starting Quantity	SQ Mean	SQ Std. Dev.
H07	SYBR	Unkn	DPBS	24	2.462E+00	0.391	2.46E+00	0.00E+00
H08	SYBR	Unkn	DPBS	24	0	0	0	0
D09	SYBR	Unkn	DV-20 Total	28	5.066E+03	3.705	5.04E+03	3.08E+01
D10	SYBR	Unkn	DV-20 Total	28	5.022E+03	3.701	5.04E+03	3.08E+01
A09	SYBR	Unkn	Omega 10 K Total	25	2.478E+04	4.394	2.50E+04	3.36E+02
A10	SYBR	Unkn	Omega 10 K Total	25	2.525E+04	4.402	2.50E+04	3.36E+02
A03	SYBR	Unkn	Omega 300VR - 110	1	1.605E+04	4.205	2.33E+04	1.03E+04
A04	SYBR	Unkn	Omega 300VR – 110	1	3.056E+04	4.485	2.33E+04	1.03E+04

B03	SYBR	Unkn	Omega 300VR - 120	2	2.800E+04	4.447	2.99E+04	2.75E+03
B04	SYBR	Unkn	Omega 300VR - 120	2	3.189E+04	4.504	2.99E+04	2.75E+03
C03	SYBR	Unkn	Omega 300VR - 130	3	2.497E+04	4.397	3.15E+04	9.24E+03
C04	SYBR	Unkn	Omega 300VR - 130	3	3.804E+04	4.580	3.15E+04	9.24E+03
D03	SYBR	Unkn	Omega 300VR - 140	4	2.287E+04	4.359	2.33E+04	5.42E+02
D04	SYBR	Unkn	Omega 300VR - 140	4	2.363E+04	4.374	2.33E+04	5.42E+02
E03	SYBR	Unkn	Omega 300VR - 150	5	3.680E+04	4.566	3.14E+04	7.68E+03
E04	SYBR	Unkn	Omega 300VR - 150	5	2.594E+04	4.414	3.14E+04	7.68E+03
F09	SYBR	Unkn	Omega 300VR Total	30	2.297E+04	4.361	2.77E+04	6.70E+03
F10	SYBR	Unkn	Omega 300VR Total	30	3.244E+04	4.511	2.77E+04	6.70E+03
C09	SYBR	Unkn	PBGC 1 Total	27	4.777E+04	4.679	4.75E+04	4.25E+02
C10	SYBR	Unkn	PBGC 1 Total	27	4.717E+04	4.674	4.75E+04	4.25E+02
F03	SYBR	Unkn	PBGC 2 - 10	6	4.797E+04	4.681	7.13E+04	3.30E+04
F04	SYBR	Unkn	PBGC 2 - 10	6	9.457E+04	4.976	7.13E+04	3.30E+04
G05	SYBR	Unkn	PBGC 2 - 100	15	6.658E+04	4.823	6.44E+04	3.02E+03
G06	SYBR	Unkn	PBGC 2 - 100	15	6.231E+04	4.795	6.44E+04	3.02E+03
H05	SYBR	Unkn	PBGC 2 - 110	16	4.939E+04	4.694	6.55E+04	2.28E+04
H06	SYBR	Unkn	PBGC 2 - 110	16	8.163E+04	4.912	6.55E+04	2.28E+04
A07	SYBR	Unkn	PBGC 2 - 120	17	3.812E+04	4.581	4.33E+04	7.28E+03
A08	SYBR	Unkn	PBGC 2 - 120	17	4.841E+04	4.685	4.33E+04	7.28E+03
B07	SYBR	Unkn	PBGC 2 - 130	18	4.792E+04	4.681	5.08E+04	4.10E+03
B08	SYBR	Unkn	PBGC 2 - 130	18	5.373E+04	4.730	5.08E+04	4.10E+03
C07	SYBR	Unkn	PBGC 2 – 140	19	5.133E+04	4.710	6.02E+04	1.25E+04

C08	SYBR	Unkn	PBGC 2 - 140	19	6.903E+04	4.839	6.02E+04	1.25E+04
D07	SYBR	Unkn	PBGC 2 - 150	20	4.304E+04	4.634	4.94E+04	9.05E+03
D08	SYBR	Unkn	PBGC 2 - 150	20	5.584E+04	4.747	4.94E+04	9.05E+03
G03	SYBR	Unkn	PBGC 2 - 20	7	4.766E+04	4.678	5.07E+04	4.27E+03
G04	SYBR	Unkn	PBGC 2 - 20	7	5.369E+04	4.730	5.07E+04	4.27E+03
H03	SYBR	Unkn	PBGC 2 - 30	8	4.652E+04	4.668	5.51E+04	1.21E+04
H04	SYBR	Unkn	PBGC 2 - 30	8	6.365E+04	4.804	5.51E+04	1.21E+04
A05	SYBR	Unkn	PBGC 2 - 40	9	5.006E+04	4.699	4.30E+04	1.00E+04
A06	SYBR	Unkn	PBGC 2 - 40	9	3.588E+04	4.555	4.30E+04	1.00E+04
B05	SYBR	Unkn	PBGC 2 - 50	10	5.585E+04	4.747	5.65E+04	9.06E+02
B06	SYBR	Unkn	PBGC 2 - 50	10	5.713E+04	4.757	5.65E+04	9.06E+02
C05	SYBR	Unkn	PBGC 2 - 60	11	5.094E+04	4.707	5.05E+04	6.72E+02
C06	SYBR	Unkn	PBGC 2 - 60	11	4.999E+04	4.699	5.05E+04	6.72E+02
D05	SYBR	Unkn	PBGC 2 - 70	12	5.885E+04	4.770	7.32E+04	2.03E+04
D06	SYBR	Unkn	PBGC 2 - 70	12	8.761E+04	4.943	7.32E+04	2.03E+04
E05	SYBR	Unkn	PBGC 2 - 80	13	5.366E+04	4.730	5.60E+04	3.29E+03
E06	SYBR	Unkn	PBGC 2 - 80	13	5.832E+04	4.766	5.60E+04	3.29E+03
F05	SYBR	Unkn	PBGC 2 - 90	14	6.929E+04	4.841	6.94E+04	1.38E+02
F06	SYBR	Unkn	PBGC 2 - 90	14	6.949E+04	4.842	6.94E+04	1.38E+02
G09	SYBR	Unkn	PBGC 2 Total	31	3.991E+04	4.601	4.45E+04	6.43E+03
G10	SYBR	Unkn	PBGC 2 Total	31	4.901E+04	4.690	4.45E+04	6.43E+03
B09	SYBR	Unkn	RVRM Total	26	3.589E+04	4.555	3.80E+04	3.04E+03
B10	SYBR	Unkn	RVRM Total	26	4.019E+04	4.604	3.80E+04	3.04E+03
A01	SYBR	Std	Standard 1	1	1.000E+02	2.000	1.00E+02	0.00E+00
A02	SYBR	Std	Standard 1	9	1.000E+02	2.000	1.00E+02	0.00E+00
B01	SYBR	Std	Standard 2	2	1.000E+03	3.000	1.00E+03	0.00E+00
B02	SYBR	Std	Standard 2	10	1.000E+03	3.000	1.00E+03	0.00E+00
C01	SYBR	Std	Standard 3	3	1.000E+04	4.000	1.00E+04	0.00E+00
C02	SYBR	Std	Standard 3	11	1.000E+04	4.000	1.00E+04	0.00E+00
D01	SYBR	Std	Standard 4	4	1.000E+05	5.000	1.00E+05	0.00E+00
D02	SYBR	Std	Standard 4	12	1.000E+05	5.000	1.00E+05	0.00E+00
E01	SYBR	Std	Standard 5	5	1.000E+06	6.000	1.00E+06	0.00E+00
E02	SYBR	Std	Standard 5	13	1.000E+06	6.000	1.00E+06	0.00E+00
F01	SYBR	Std	Standard 6	6	1.000E+07	7.000	1.00E+07	0.00E+00
F02	SYBR	Std	Standard 6	14	1.000E+07	7.000	1.00E+07	0.00E+00
G01	SYBR	Std	Standard 7	7	1.000E+08	8.000	1.00E+08	0.00E+00
G02	SYBR	Std	Standard 7	15	1.000E+08	8.000	1.00E+08	0.00E+00
H01	SYBR	Std	Standard 8	8	1.000E+09	9.000	1.00E+09	0.00E+00

H02	SYBR	Std	Standard 8	16	1.000E+09	9.000	1.00E+09	0.00E+00
E07	SYBR	Unkn	Stock 11/10/08	21	3.776E+04	4.577	4.62E+04	1.19E+04
E08	SYBR	Unkn	Stock 11/10/08	21	5.456E+04	4.737	4.62E+04	1.19E+04
G07	SYBR	Unkn	Stock 12/10/08 #2	23	5.074E+04	4.705	5.83E+04	1.07E+04
G08	SYBR	Unkn	Stock 12/10/08 #2	23	6.585E+04	4.819	5.83E+04	1.07E+04
F07	SYBR	Unkn	Stpcl 12/10/08	22	4.873E+04	4.688	8.04E+04	4.48E+04
F08	SYBR	Unkn	Stpcl 12/10/08	22	1.121E+05	5.050	8.04E+04	4.48E+04
E09	SYBR	Unkn	VP Total	29	2.152E+04	4.333	2.52E+04	5.23E+03
E10	SYBR	Unkn	VP Total	29	2.891E+04	4.461	2.52E+04	5.23E+03

Appendix II: Gigantic Magnetoresistive (GMR) Sensor

Introduction:

Efficient methods are needed to detect and count magnetic nanoparticle viral surrogates (MNPVS). Reported here, is the development of a MNPVS assay chip based on spin-valve bridges. Each leg of the sensor consists of a series parallel array of 1 μm wide x 1 mm long elements. The sensor resistance is approximately 30 kΩ. A 0.5μl drop of nanoparticles suspended in water is pipetted onto one bridge element of the bridge. The nanoparticles change the effective permeability of one leg, increasing its resistance change in an applied AC field. A voltage output is then created which is proportional to the number of nanoparticles on the sensor. Initial measurements indicate that 10^4 particles can be detected in 0.5μl. Given a magnetic concentration factor of 10^5, this technique can lead to the detection of 2×10^5 particles per liter. Spin-valve technology can also be used to develop nanoparticle scanners which operate in a similar fashion to read heads. These scanners can be used to interrogate the density of MNPVS on the surface of filtration membranes.

Experimental Methods:

Design:

The following designs for the GMR sensors were developed by Stephen Russek of the Magnetics Group at the National Institute of Standards and Technology (NIST) using Whiteley Research, Inc. Design Software.

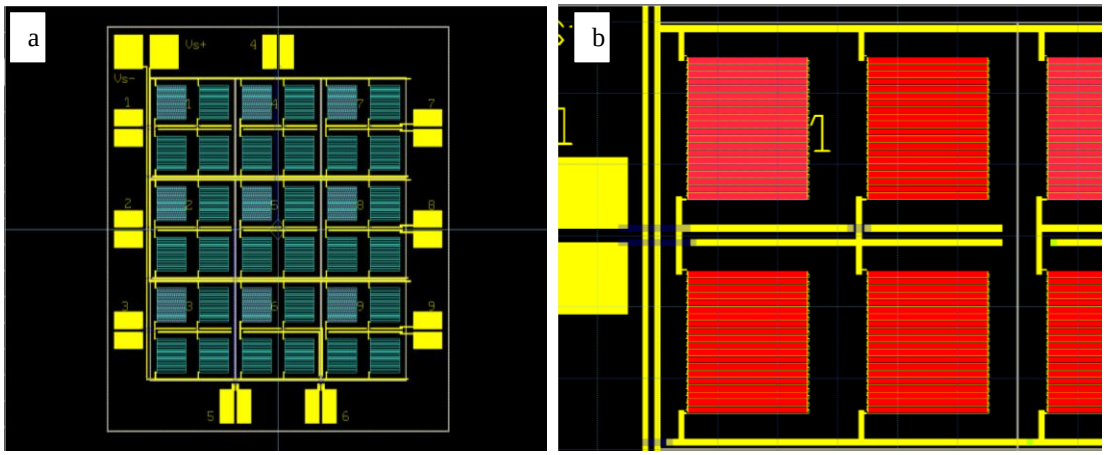

Figure 12. (a) GMR assay design, where the yellow color indicates the first electrode layer, the green color indicates the VIA layer, and the blue color is the second electrode layer. The white square indicates a size of 12mm x 12mm. (b) GMR assay design, enlarged, where the red color indicates the GMR layer. The white square indicates a size of 1mm x 1mm.

This sensor design is comprised of a 3X3 grid, for a total of 9 assay squares that are enlarged in Figure 12 (b). The assay square labeled "1" contains 1µm wide GMR sensors, spaced 1µm apart (in red). There are three additional GMR sensors located in close proximity to the assay well, serving to measure a change in resistance. The purpose of this design is to be able to make serial dilutions of nanoparticle permeate (after filtration), and pipette each of 9 dilutions into one well of the assay chip. This will help to identify a limit of detection for these GMR devices, especially when working with high concentrations of nanoparticles (i.e., 10^8 particles/ml).

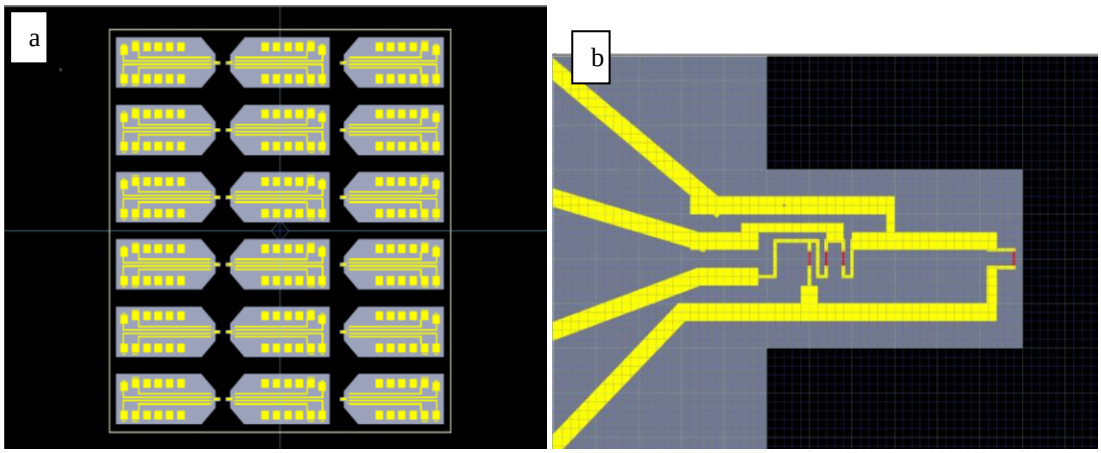

Figure 13. (a) GMR scanner design, where the gray color indicates the dielectric layer and yellow is the first electrode layer. The white square indicates a size of 12mm x 12mm. (b) GMR scanner design, enlarged, where the red color indicates the GMR layer. The tiny, red GMR layers are 1µm wide.

This sensor design consists of an approximately 1-2µm long and 500 nm wide gigantic magnetoresistive (GMR) device (in red) located at the tip of the device. The three additional GMR sensors located directly behind the tip are references sensors to act as a bridge to sense the change in resistance when the tip recognizes a magnetic nanoparticle. The goal of this design is to be able to scan the GMR tip across a membrane, or other surface, containing magnetic nanoparticles, and thereby quantify the amount of particles on the membrane.

Substrates and Deposition:

Three inch, 1-10 Ohm-cm silicon wafers with 150nm SiO2 were deposited with the following elements using a 150 Oe magnetic field aligned parallel to the flat of the wafer and a 12A magnetic current at 2.3V:

Element	Deposition Thickness (Angstroms)
Ta	50
NiFe (80/20)	40
Co	10
Cu	27
Co	18

Ru	6
Co	15
IrMn	100
Ta	40

The wafers were given the following identifications: SV9-26-03A, SV9-26-03B, and SV-9-29-03C.

Photomasks (Reticles):

The masks were developed with CD-26 developer for approximately 60 seconds, rinsed in DI water, dried with nitrogen, and examined under a compound microscope for defects. The masks were then etched with a weak acid, CR-75, for approximately 2 minutes, then rinsed with DI water and examined under the compound microscope. The photoresist was stripped in an ultrasonicator for 3-5 minutes, rinsed and returned to the ultrasonicator for approximately 3 minutes. The masks were then cleaned.

Base Layer Photolithography:

Lift off resist (LOR1A) was spun onto the spin valve at 2500RPM for 40 seconds, and baked at 150°C for 4 minutes. SPR660 resist was spun on at 3200RPM for 35 seconds, followed by a 60 second bake at 95°C. The wafer was exposed on the Stepper at 220 mJ/cm^2, using the GMR mask designs described previously. The wafer was baked for 60 seconds at 110°C post exposure, followed by a developing step for 60 seconds in MF701 or MF26a developer. The wafer was rinsed with DI water and examined under the compound microscope for defects. The wafer was baked for an additional 60 seconds at 95°C.

Base Layer Etch:

The base layer of the wafer was ion beam etched in the Intelvac chamber using the following parameters:

Unit	Parameter
Ic	8.0 A

V_d(V)	40
Vb	200V
V_a(V)	100
I_d(A)	0.43
I_b(mA)	30
Ia	1mA
I_{ne}(mA)	50
I_n(A)	6.4
Ip	0.13 mA/cm^2
Air flow	7.5 sccm
P	3.0e-4T
Time	10 min
Temp	90°C

The wafer was ultrasonicated in PG remover for 20 minutes, followed by ultrasonication in isopropanol for 3 minutes. The etch thickness was measured by the Ambios profilometer.

Electrode 1 Photolithography:

Lift off resist (LOR3A) was spun onto the spin valve at 2500RPM for 40 seconds, and baked at 150°C for 4 minutes. SPR660 resist was spun on at 3200RPM for 35 seconds, followed by a 60 second bake at 95°C. The wafer was exposed on the Stepper at 245 mJ/cm^2, using the electrode mask designs described previously. The wafer was baked for 60 seconds at 110°C post exposure, followed by a developing step for 60 seconds in MF701 or MF26a developer. The wafer was rinsed with DI water and examined under the compound microscope for defects. The wafer was baked for an additional 60 seconds at 95°C.

Electrode 1 Deposition:

The wafer was cleaned via ion beam in the Intelvac chamber using the following parameters:

Unit	Parameter
Ic	8.0 A
V_d(V)	40
Vb	300V
V_a(V)	200
I_d(A)	0.43
I_b(mA)	40
Ia	5mA
I_{ne}(mA)	50
I_n(A)	6.74
Ip	0.13 mA/cm^2
Air flow	7.5 sccm
P	2.8e-4T
Time	0.5 min
Temp	90°C

120nm gold/copper was deposited on the wafer in the Intelvac chamber at 22nm per minutes using the following parameters:

Unit	Parameter
Ic	8.0 A
V_d(V)	40
Vb	1000V
V_a(V)	100
I_d(A)	0.43
I_b(mA)	55
Ia	5mA

I_{ne}(mA)	50
I_n(A)	6.74
Air flow	7.5 sccm
P	3.0e-4T
Time	6.05 min
Temp	90°C

The wafer was ultrasonicated in PG remover for 30 minutes, followed by ultrasonication in isopropanol for 3 minutes. The gold electrode layer thickness was measured by the Ambios profilometer.

Note: SV9-29-03C was processed through electrode layer 1 deposition, then diced and tested. SV9-26-03A was processed entirely, and SV9-26-03B was not processed.

SiNx 1 Deposition:

Silicon nitride was deposited on SV9-26-03A in the Lesker chamber in order to allow the area of the GMR assay sensor outside of the wells to be more hydrophobic so as to target magnetic nanoparticle solution to the assay wells. SiNx was sputtered for 30 minutes to achieve approximately a 100nm thickness. The SiNx layer thickness was measured by the Ambios profilometer.

Via 1 Photolithography:

SPR660 was spun onto the spin valve at 3200RPM for 35 seconds, and baked at 95°C for 60 seconds. The wafer was exposed on the Stepper at 270 mJ/cm^2, using the VIA mask designs described previously. The wafer was baked for 60 seconds at 110°C post exposure, followed by a developing step for 60 seconds in MF701 or MF26a developer. The wafer was rinsed with DI water and examined under the compound microscope for defects.

Via 1 Etch:

The AXIC etcher was used to perform the Via 1 etch. The following parameters were used:

Unit	Parameter
O2	2 sccm
CF4	42 sccm
Watts	75
Voltage	-200
Time	400 seconds
Depth	Electrode: 80nm SiO_2: 100nm

Electrode 2 Photolithography:

Lift off resist (LOR3A) was spun onto the spin valve at 2500RPM for 40 seconds, and baked at 150°C for 4 minutes. SPR660 resist was spun on at 3200RPM for 35 seconds, followed by a 60 second bake at 95°C. The wafer was exposed on the Stepper at 245 mJ/cm^2, using the second electrode mask designs described previously. The wafer was baked for 60 seconds at 110°C post exposure, followed by a developing step for 60 seconds in MF701 or MF26a developer. The wafer was rinsed with DI water and examined under the compound microscope for defects.

Electrode 2 Deposition:

The wafer was cleaned via ion beam in the Intelvac chamber using the following parameters:

Unit	Parameter
Ic	8.0 A
V_d(V)	40
Vb	300V
V_a(V)	400

I_d(A)	0.43
I_b(mA)	40
Ia	5mA
I_{ne}(mA)	50
I_n(A)	6.74
Ip	0.13 mA/cm^2
Air flow	7.5 sccm
P	2.8e-4T
Time	0.5 min
Temp	90°C

160nm gold/copper was deposited on the wafer in the Intelvac chamber at 8nm per minutes using the following parameters:

Unit	**Parameter**
Ic	8.0 A
V_d(V)	40
Vb	1000V
V_a(V)	100
I_d(A)	0.43
I_b(mA)	60
Ia	5mA
I_{ne}(mA)	70
I_n(A)	6.74
Air flow	7.5 sccm
P	2.8e-4T
Time	20 min

Temp	90°C

The wafer was ultrasonicated in PG remover for 30 minutes, followed by ultrasonication in isopropanol for 3 minutes. The gold electrode layer thickness was measured by the Ambios profilometer.

Deep Reactive Ion Etching (RIE):

SPR220 7.0 was spun on at 2700RPM for 45 seconds, followed by a 100 second bake at 95°C and another bake at 115°C for 100 seconds. The wafer was allowed to sit in air for no less than one hour. The wafer was exposed at 2000 mJ/cm^2 and developed for 60 seconds, as described previously. SiO_2 was removed in the AXIC etcher using a pre-programmed recipe to etch 150nm in approximately 17 minutes. The wafer was waxed by placing a dummy wafer on a 150°C hotplate and applying wax. SV9-26-03A was mounted on the dummy and both were removed from the hotplate and allowed to cool. The wafer was etched using a pre-programmed cycle, and removed from backing.

Atomic Force Microscopy (AFM):

Scanning probe microscope images were taken using the Veeco EnviroScope.

Results and Discussion:

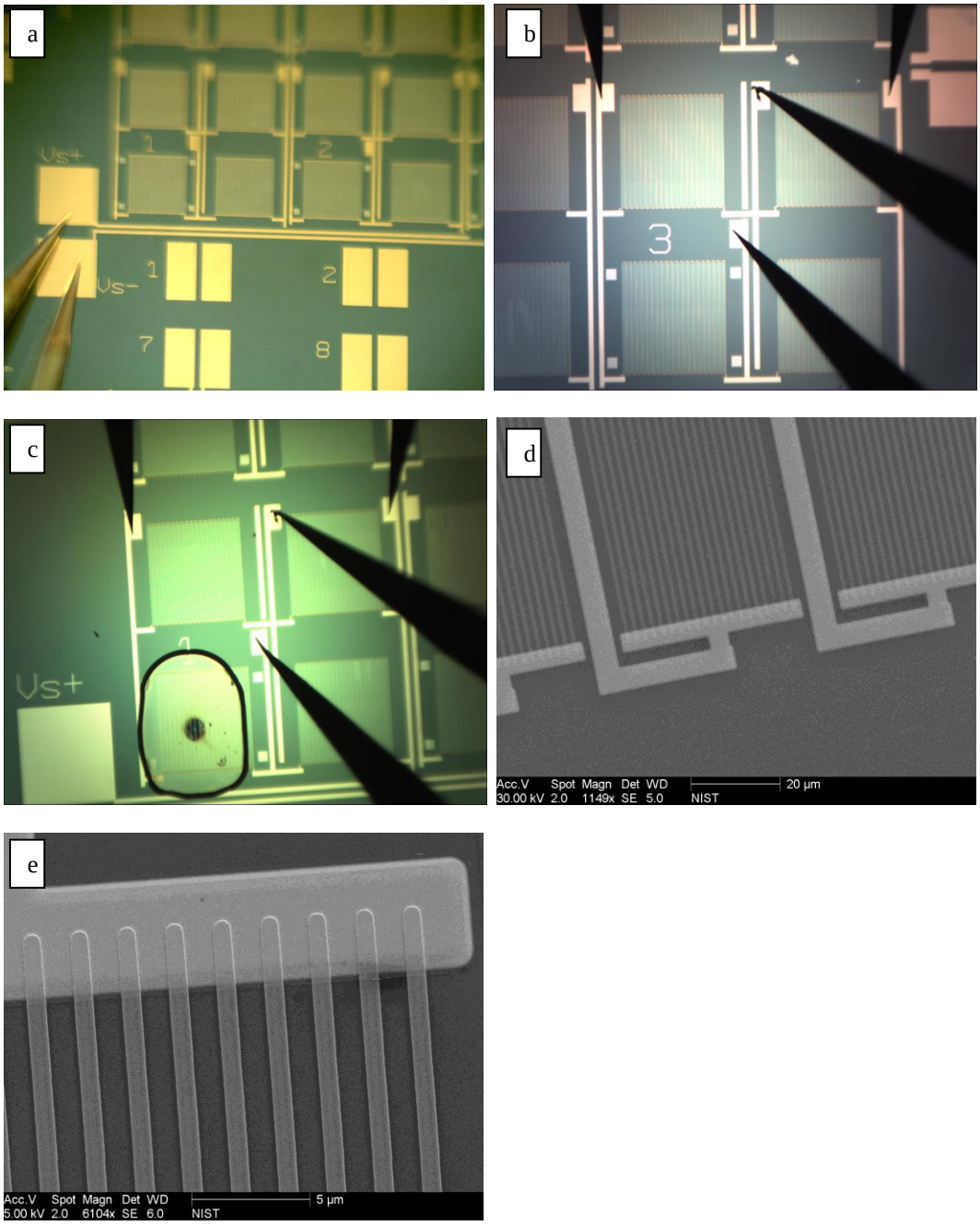

Figure 14. (a) MNPVS assay prototype showing the probe tips at the voltage output. (b) Enlarged view of a single well showing all probe tips measuring the change in voltage. (c) Assay well after the addition of 500µl of commercially available magnetic nanoparticle solution. (d) Magnification (1149x) of the GMR wires within each assay well. (e) Further magnification (6104x) of the GMR wires within the assay well.

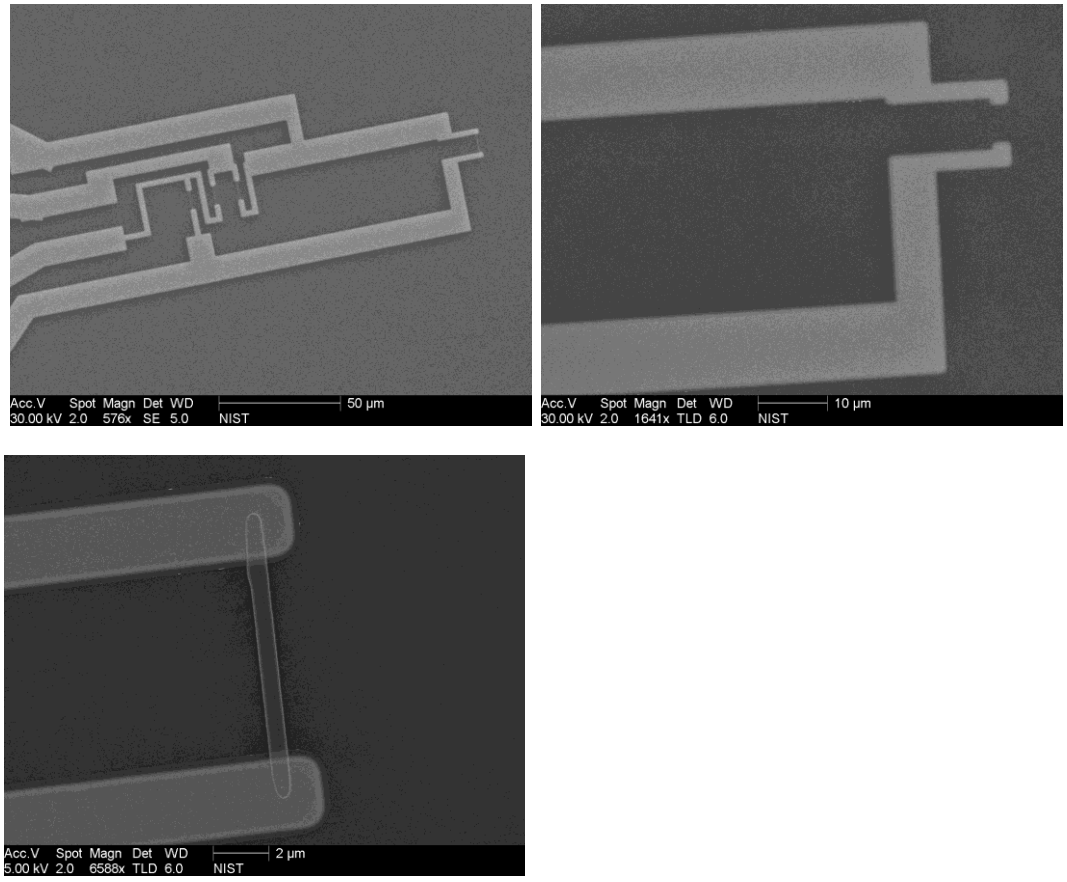

Figure 15. (a) Magnification (576x) of the MNPVS scanner prototype. (b) Further magnification (1641x) of the scanner showing a defect in the mask design with a missing the GMR wire. (c) Magnification (6588x) of the scanner showing an intact GMR wire.

Images were taken to observe for defects in the mask designs. Several defects existed, as demonstrated by figure 14 (b). Figure 13 (c) demonstrates the behavior of the nanoparticle solution. As a drop of solution, 500µl in volume, is applied, nanoparticles are clustering toward the center of the well.

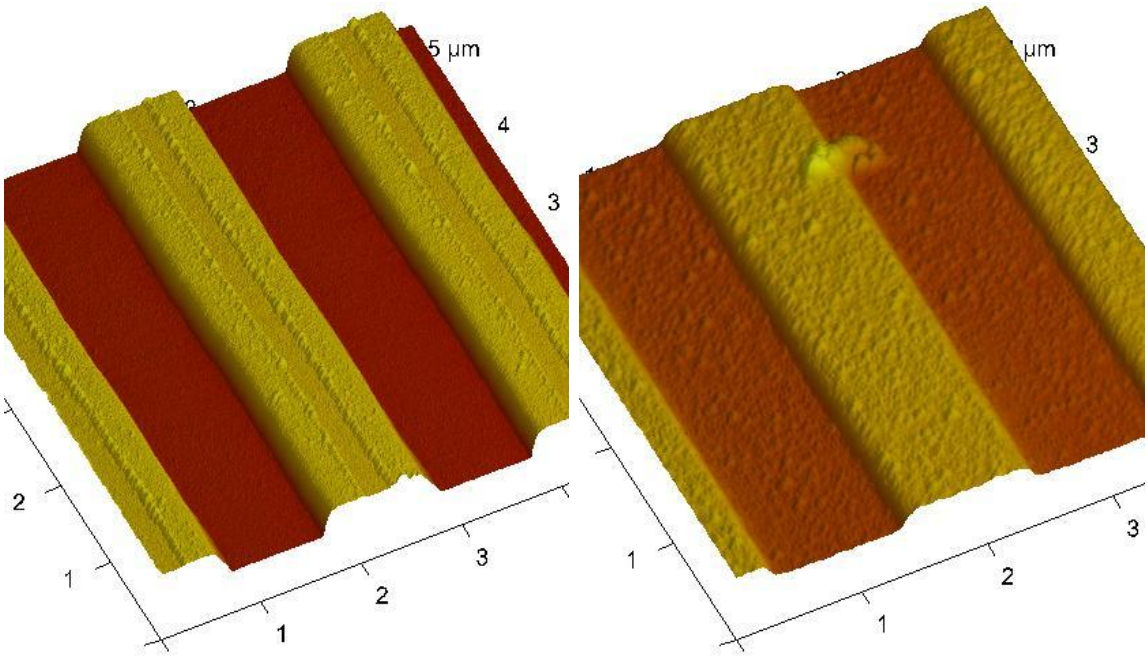

Figure 16. (Left) Atomic force micrograph of the 1 µm lines/spacings within an assay well without nanoparticles applied. (Right) Atomic force micrograph of the 1 µm lines/spacings with Molday Ion C6 Amine nanoparticles applied.

Magnetic nanoparticles are clumping on the surface of the assay well. This poses problems for future development of the scanning device, that will ultimately rely on single particles for detection.

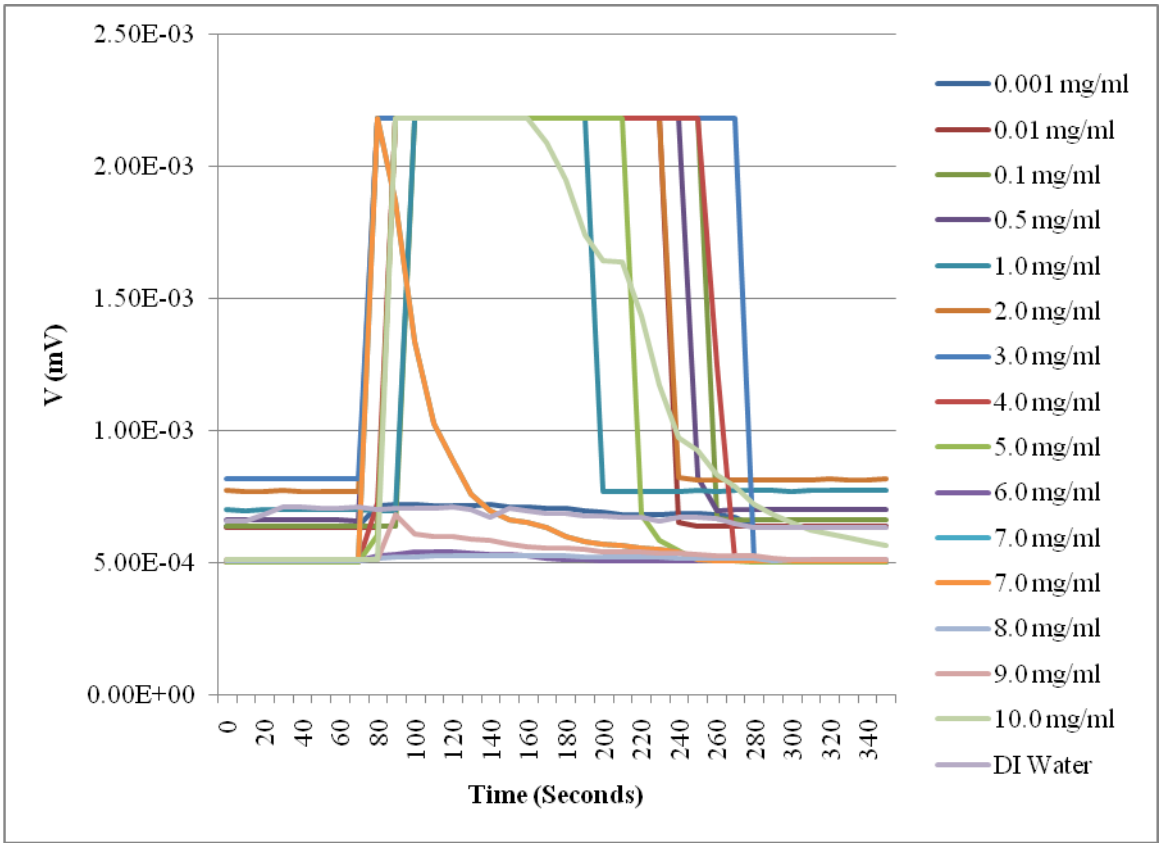

Figure 17. Voltage Output During Application of Various Concentrations of Iron Oxide Nanoparticles

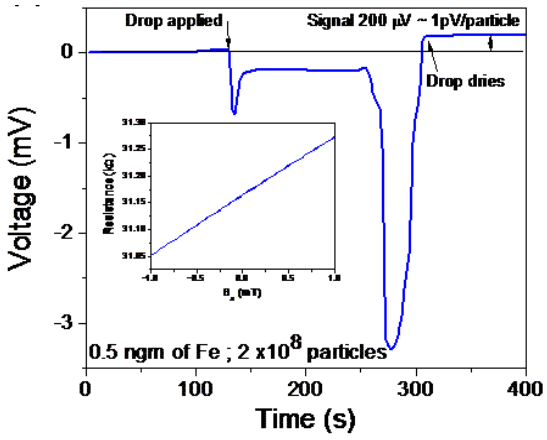

Figure 18. Voltage output during application of 2 x 10^8 iron oxide nanoparticles. The inset shows the magnetoresistive response of the sensor.

The sensor signal becomes saturated with increased concentration of nanparticles. There is a large change in signal that can be attributed to a change in temperature (from the temperature of the sensor, to the temperature of the drop applied), followed by evaporation of the liquid in the drop. Applying the drop of solution changes the capacitance, inductance, and dielectric constant within the well.

Conclusions:

The first prototype of both a GMR assay and a GMR scanner device for detection of magnetic nanoparticles has been developed. Only the GMR assay has been tested, but has lead to many insights on the further optimization and development of the sensor. Parameters such as developing time, bake time and temperature, annealing, and deposition can be adjusted to enhance the performance and level of detection of the sensor. Additionally, the sensor signal obtained depends on parameters such as the nanoparticle:GMR sensor size ratio, the magnetic moment of the particle, the distance between the particle and the sensing layer, temperature, and particle dispersion, among others. Further optimization will include evaluating the solution in which the particles are applied, developing and using a standard nanoparticle across all testing, adding additional hydrophobic layers to areas on the sensor other than the assay wells to help contain the drop within a well, and further analyzing the sensor for defects in order to correct them.

Appendix III: Constant Flux Filtration

Introduction:

Constant flux filtration has been used to minimize fouling during filtration processes, particularly for sterile filtration. As opposed to constant pressure filtration, constant flux filtration can decrease the rate of fouling that occurs. In order to maintain a constant flux, typically large increases in transmembrane pressure are required to offset membrane fouling (Ho & Zydney, 2002). Constant flux filtration experiments can provide further insight into the virus rejection properties of membranes when run in different operational modes, which can further be used as a metric for comparing live virus to virus surrogates.

Experimental Methods:

Filtration experiments were conducted using feed streams consisting of low protein solutions containing 10^8 virus particles/ml as described previously. The solution was filtered in a standard 200ml, model 8200 Amicon stirred cell (Millipore, Billerica, MA) in normal (dead-end) filtration mode at a constant pressure of 30psi (0.2 MPa) in a biological safety cabinet. Constant flux was regulated by a Master Flex peristaltic pump (Cole-Parmer, Vernon Hills, IL). For the DV 20 membrane, constant flux was regulated at 40 LMH, as this is the typical pure water permeance value for this membrane at 30 PSI. The Omega 10 and PBGC membranes were operated at a constant flux of 200 LMH, as this value was the maximum flux of the peristaltic pump, and the closest value to their typical pure water permeances. The other three membranes, described previously, were not included in this set of experiments due to limitations in maximum flux. Samples were collected and analyzed as described previously for virus quantification.

Results and Discussion:

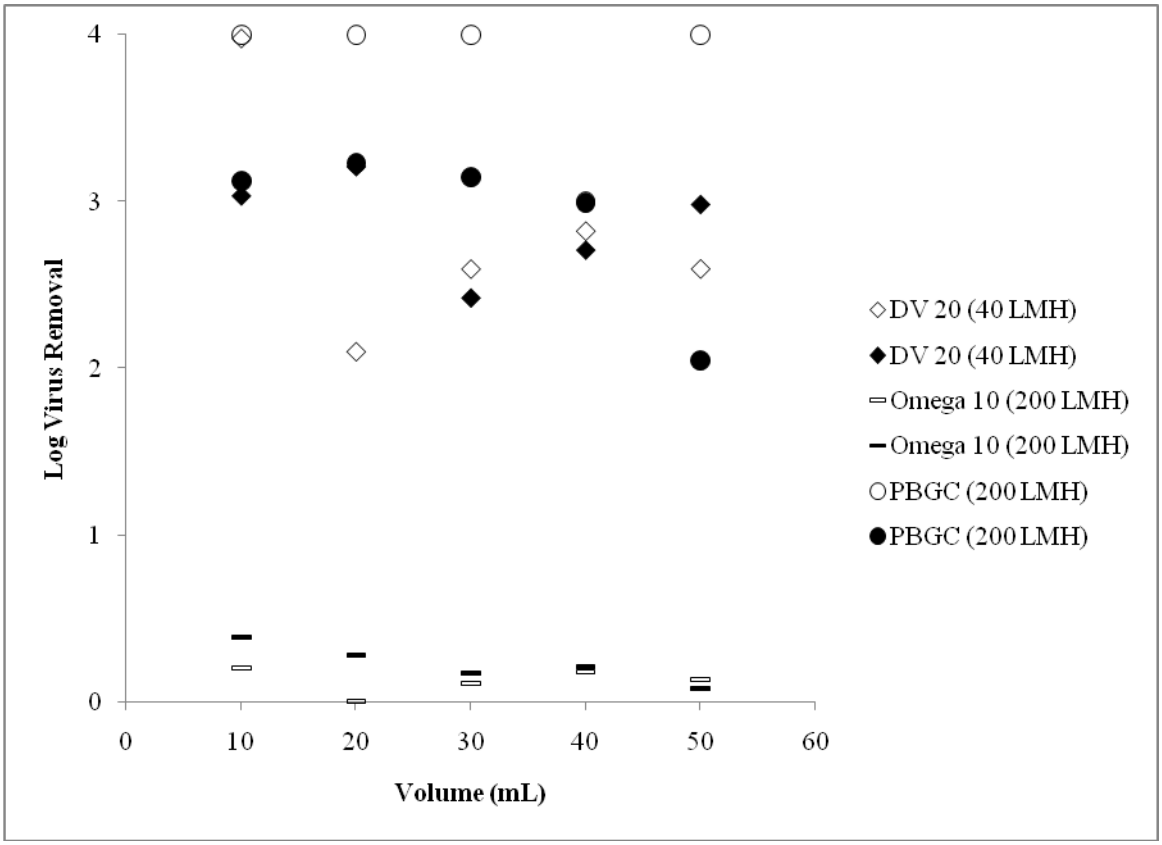

Figure 19. Log Virus Removal for 30 PSI Constant Pressure Filtration (open symbols) and Constant Flux Filtration (filled symbols) of Feed Streams Spiked with MVM Not Containing Protein

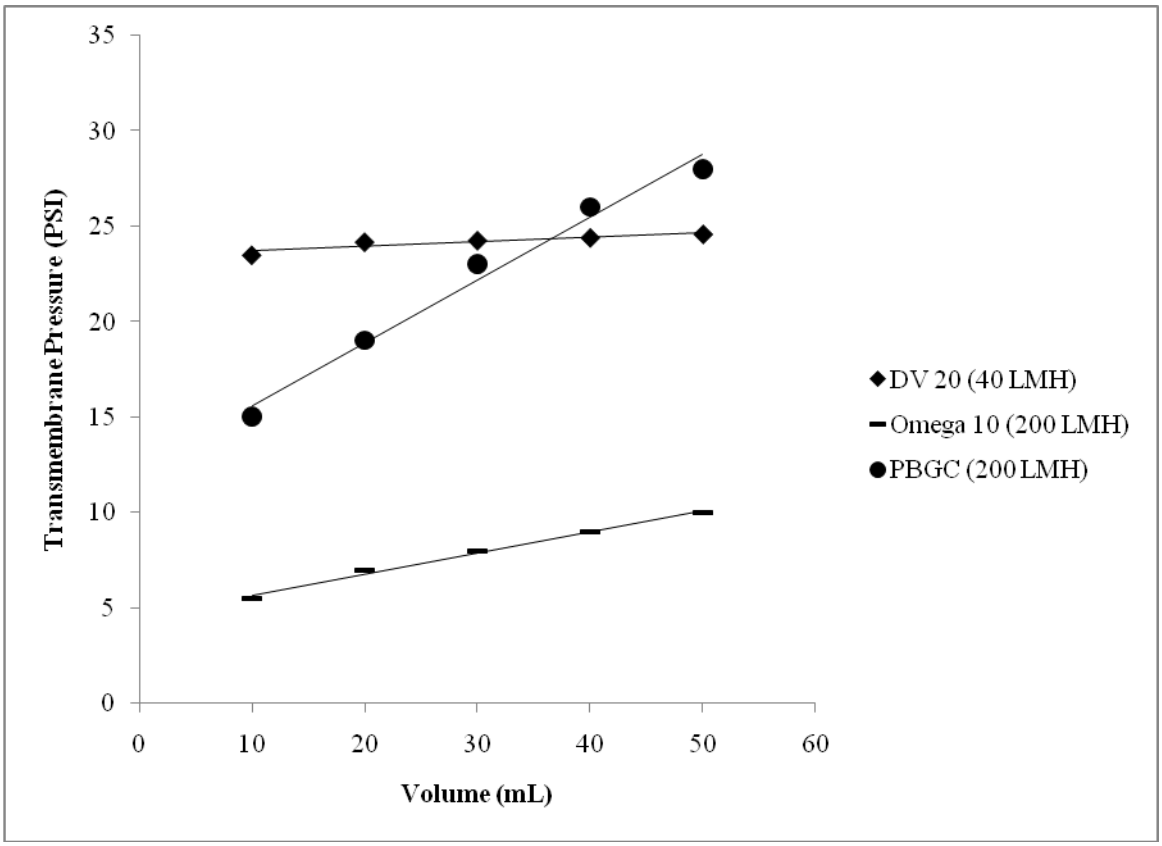

Figure 20. Transmembrane Pressures for Constant Flux Filtration of Feed Streams Spiked with MVM Not Containing Protein

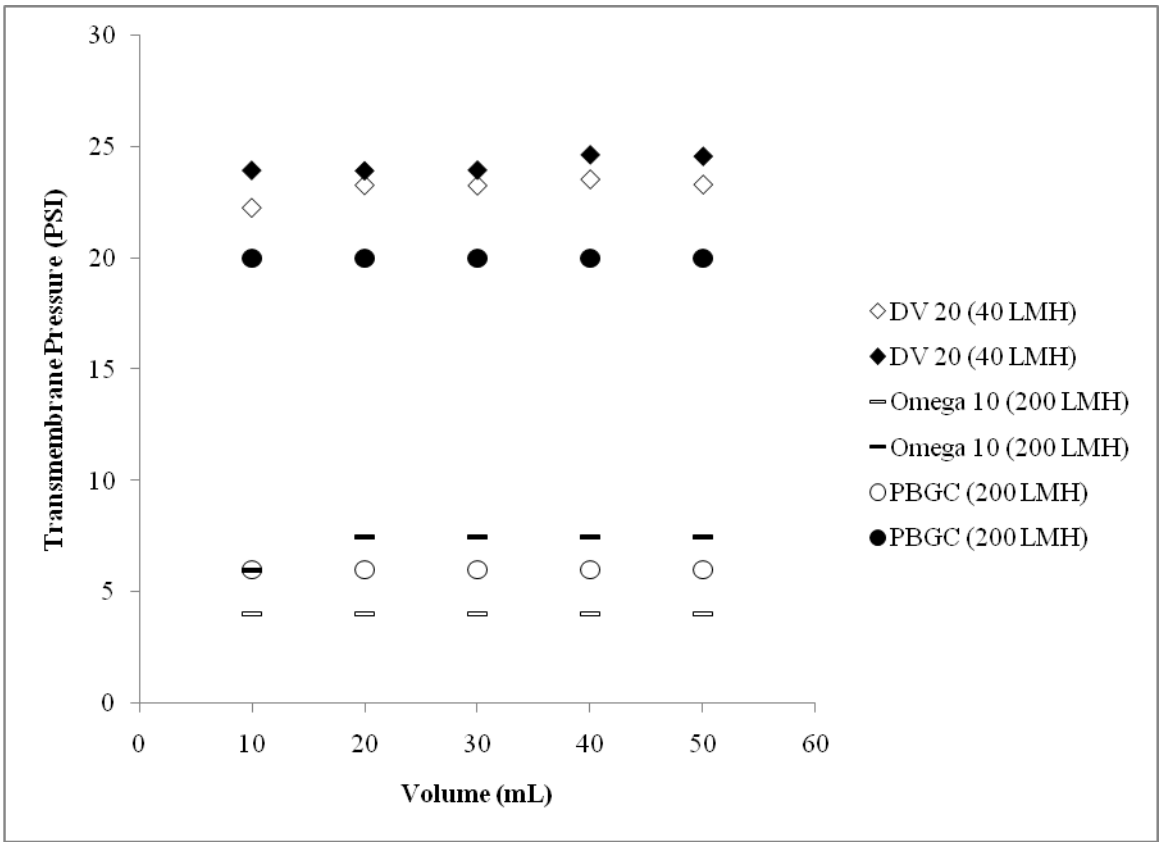

Figure 21. Comparison of Transmembrane Pressure Before Filtration (open symbols) and After Filtration with Feed Streams Spiked with MVM Not Containing Protein (filled symbols)

Conclusions:

Log virus removal during constant flux filtration of feed streams not containing protein was similar to that observed during constant pressure filtration, except for the PBGC membrane. The PBGC membrane experienced a lower reduction in virus during constant flux filtration as opposed to constant pressure filtration. This lessened viral clearance could be attributed to the increase in transmembrane pressure observed during filtration that could have forced virus particles through those pores on the large end of the pore size distribution.

Further studies comparing live virus and virus surrogate removal during constant flux filtration should be conducted in order to provide more supporting data that surrogates behave as live virus. Additionally,

experiments using model proteins, such as BSA, with virus will also provide useful data to use for comparison.